Supplementary Information for

Amyloid–Nucleotide Interactions Promote Prebiotic ATP Synthesis

Saroj K. Rout[1*], Nina Wehr[2], Riccardo Cadalbert[1], Julian Stropp[1], David Rhyner[1], Harindranath Kadavath[1], Peter Güntert[3], Daniel Klose[1], Thomas Wiegand[2], Jason Greenwald[1], Roland Riek[1*]

[1] Institute of Molecular Physical Science, Department of Chemistry and Applied Biosciences, ETH Zurich, 8093 Zurich, Switzerland

[2] Institute of Technical and Macromolecular Chemistry, RWTH Aachen University, 52074 Aachen, Germany; Max Planck Institute for Chemical Energy Conversion, 45470 Mülheim a. d. Ruhr, Germany

[3] Institute of Molecular Physical Science, Department of Chemistry and Applied Biosciences, ETH Zurich, 8093 Zurich, Switzerland; Institute of Biophysical Chemistry, Goethe University, 60438 Frankfurt am Main, Germany; Department of Chemistry, Tokyo Metropolitan University, Hachioji 192-0397, Japan

* Email: saroj.rout@phys.chem.ethz.ch; roland.riek@phys.chem.ethz.ch

Materials and Methods

Peptide manipulations

The peptides, synthesized using standard Fmoc chemistry, were purchased from GLS China as either pure or crude compounds. The crude peptides were purified by reverse-phase HPLC on a Kinetex C18 5 µm 10×250 mm column (Phenomenex) in either CH_3CN/H_2O/TFA or CH_3CN/H_2O/TEAA solvent systems. The quantitation of the peptides was performed by reverse-phase HPLC and was based on their calculated extinction coefficient at 214 nm [1,2]. Pure peptides were aliquoted, lyophilized, and stored at −20 °C until use.

Fibrillization

Lyophilized peptides were dissolved in water or DMSO at concentrations >5 mM and subsequently diluted to 100–200 µM in buffers of the desired pH (citrate–phosphate, acetate, or phosphate). Samples were incubated overnight at room temperature in a thermomixer (Eppendorf) at 1000 rpm to promote fibril formation. For experiments requiring higher peptide concentrations, aggregates were pelleted by centrifugation (25,000g for 30 min) and resuspended in the desired buffer to yield final concentrations of 1–2 mM peptide amyloids. The final DMSO concentration in all samples was <1% (v/v).

Amyloid-nucleotide binding assays

Nucleotides (ATP, GTP, UTP, CTP, ADP) were purchased at ≥99% purity (Sigma-Aldrich) and dissolved in ultrapure water. Amyloid aggregates and nucleotides were mixed in DNA LoBind® tubes (Eppendorf) at desired concentrations in citrate–phosphate buffer (pH 3 or 5) or phosphate buffer (pH 7). Samples were incubated overnight at room temperature, followed by centrifugation **(**25,000g for 1 h) to separate bound and unbound fractions. The supernatant was analyzed by reverse-phase HPLC in CH_3CN/H_2O/TEAA solvent systems using a BioZen C18 or BioZen Oligo C18 column (2.6 µm, 4.6 × 150 mm, Phenomenex) connected to an Agilent 1200 system equipped with a diode array detector. The samples injected onto the column were resolved using a linear gradient of acetonitrile (0–15%) at a flow rate of 1 mL/min. Detection was performed at 260 nm, and nucleotide concentrations were determined from HPLC peak areas using extinction coefficients. The amount of nucleotide bound to amyloids was calculated by subtracting the concentration in the supernatant from the total nucleotide concentration.

ATP formation from ADP and acetyl phosphate

ATP formation assays were performed by incubating ADP (Sigma-Aldrich) with Lithium potassium acetyl phosphate (AcP, Sigma-Aldrich, ≥97% purity) in the presence or absence of preformed peptide amyloids under aqueous buffered conditions. Unless otherwise specified, reactions (10 µL total volume) contained 1.2 mM ADP, 5 mM acetyl phosphate, and 1 mM peptide amyloid in either 40 mM sodium acetate buffer (pH 4–6) or 40 mM sodium phosphate buffer (pH 7). $MgCl_2$ was added where indicated to final concentrations of 5–50 mM. Acetyl

phosphate solutions were freshly prepared immediately before each experiment. Reactions were initiated by adding acetyl phosphate, mixed briefly, and incubated at room temperature for 20 h. Following incubation, 6 M guanidine hydrochloride was added to solubilize peptide aggregates. Samples were centrifuged **(**25,000g for 30 min), and the supernatants were collected for analysis. ATP formation was quantified by reverse-phase HPLC (CH_3CN/H_2O/TEAA solvent system) as described previously[2]. Product identity was independently confirmed by ^{31}P and ^{1}H NMR spectroscopy, where signals from reaction mixtures were matched to ATP standards and distinguished from ADP. Control reactions lacking peptide amyloid and/or $MgCl_2$ were analyzed in parallel. For peptide screening experiments, the peptide library included amyloidogenic sequences differing in amino acid composition and C-terminal chemistry (free acid or amidated). For pH-dependence experiments, reactions were carried out at pH 4–7 as specified. pH values refer to the initial buffer conditions before reagents are added. Absolute ATP yields varied somewhat between independent experiments, likely due to competing hydrolysis of acetyl phosphate; however, the relative trends were reproducible.

Solution-state Nuclear Magnetic Resonance (NMR) spectroscopy

Reaction mixtures and corresponding controls were supplemented with 2 M urea and 5% (v/v) D_2O before solution-state NMR measurements. One-dimensional (1D) ^{31}P NMR spectra were acquired on a Bruker Avance NEO 500 MHz spectrometer (^{31}P resonance frequency, 202.4 MHz), while 1D ^{1}H NMR spectra were recorded on a Bruker AV IIIHD 900 MHz spectrometer. The NMR data were processed and analyzed using Bruker TopSpin 4.1.4.

Solid-state Nuclear Magnetic Resonance (NMR) spectroscopy

For the solid-state NMR experiments, the peptide amyloid samples were filled into the magic-angle spinning (MAS) rotor by ultracentrifugation using filling tools developed at ETH Zurich and a Beckman Coulter Optima XPN80 ultracentrifuge at 210,000g for 30 min. The 2D ^{13}C-^{13}C DARR (Dipolar Assisted Rotational Resonance) spectrum of uniformly $^{13}C/^{15}N$ labelled VAQAQINI-NH_2 was previously published by Rout et al.[3]

For preparation of the amyloid–ATP sample, preformed peptide amyloids were incubated with ATP at pH 4, followed by centrifugation to pellet the amyloid-bound fraction. The resulting pellet was directly packed into the MAS rotor for solid-state NMR measurements. The 2D ^{13}C-^{13}C DARR spectrum (20 ms mixing time) of uniformly $^{13}C/^{15}N$ labelled VAQAQINI-NH_2: ATP was recorded at a static magnetic-field strength of 16.4 T using an MAS frequency of 17.0 kHz, and the variable temperature unit (VTU) was set to 255 K. The experiment was recorded using a Bruker Avance III console and a 3.2 mm Bruker BioSpin triple resonance “E-free” probe. All further experiments were recorded at a magnetic-field strength of 11.7 T using an MAS frequency of 17.0 kHz, and the VTU was set to 255 K. They were recorded using a Bruker Avance III HD console and a Bruker BioSpin 3.2 mm triple resonance probe. For further information on the solid-state NMR experiments, see the supporting information of the reference[3]. All spectra were referenced against 85% H_3PO_4, DSS and liquid NH_3 for ^{31}P, ^{13}C and ^{15}N respectively and processed using TopSpin 4.1.4.

To form the (^{15}N)VAQAQIN(^{13}C)I-NH_2:ADP:AcP sample with a large excess of ADP and AcP, the rotor was opened again after ultracentrifugation. A small fraction of the amyloid sample was removed from the rotor, and the rotor was filled with a solution of 0.5 M ADP and 1.36 M AcP in 0.2 M acetate buffer at pH 4. The relative amounts of ADP, AcP, and Mg^{2+} were chosen to approximate the stoichiometric ratios used in the ATP formation experiments. All relevant experimental details are given in **Table S2**.

Electron Paramagnetic Resonance (EPR) spectroscopy

Samples for W-band or Q-band EPR measurements were prepared in 40 mM acetate buffer (pH 4) containing ATP (4 mM), $MnCl_2$ (400 µM), and 30% (v/v) glycerol, either in the presence or absence of amyloid peptide VAQAQINI-NH_2 (4 mM, denoted P3 in the figures). For Q-band experiments, isotopically labelled amyloids, (^{15}N)VAQAQIN(^{13}C)I-NH_2 or (^{13}C)VAQAQIN(^{15}N)I-NH_2, denoted ^{15}N-P3 or ^{13}C-P3 respectively, were used. Samples were loaded into quartz tubes with outer diameters of 0.9 mm or 3.0 mm, for W- or Q-band experiments, respectively.

EPR experiments in W-band (ca. 94.2 GHz) were conducted on a Bruker ElexSys E680 EPR spectrometer (Bruker BioSpin, Ettlingen, Germany) upgraded with a home-built W-band microwave bridge and a 2 W solid-state microwave amplifier (QuinStar Technology, Torrance, USA). ENDOR (Electron Nuclear Double Resonance) measurements used a 150 W radiofrequency (RF) amplifier. The temperature was generally set to 10 K using a helium flow cryostat (Oxford Instruments, Oxfordshire, UK).
EPR experiments in Q-band were conducted on a home-built X/Q pulse EPR and ENDOR spectrometer equipped with two AWGs dedicated for microwave (MW) and RF pulsed excitation (see also Stropp et al.,[4] details to be published elsewhere) and a cryogen-free variable temperature EPR cryostat (Cryogenic Ltd., London, UK). For Q-band (ENDOR) operation, the spectrometer features a traveling wave tube amplifier with a nominal power of 150 W, a cavity resonator for 3.0 mm sample tubes designed with RF coils inside for ENDOR,[5] driven by a 500 W RF amplifier (Amplifier Research, Souderton, USA). Experiments in Q-band typically use an SRT of 6 ms and rectangular π/2 – π pulses of 16 – 32 ns, respectively, and a receiver video gain of -10 dB to prevent saturation of the final digitized signal, unless stated otherwise.

Davies ENDOR spectra for ^{1}H and ^{31}P were acquired with a shot repetition time (SRT) of 5 ms and with the sequence t_{inv} – T – t_p – τ – 2t_p – τ – echo, where during the time T, an RF pulse was applied followed by a delay of 10 µs to allow for RF power decay. The inversion pulse length was set to 200 ns, and the RF pulse length to 50 µs. The echo with a τ of 1 µs was integrated symmetrically around the echo maximum over a time of 1.2 µs. Due to substantial time overhead on this particular spectrometer, we used the stochastic acquisition mode with 10 shots per point. A two-step phase cycle as in EDNMR (Electron-electron double resonance (ELDOR)-detected nuclear magnetic resonance) was applied to cancel receiver offsets.

Mims ENDOR spectra for ^{31}P were acquired with an SRT of 5 ms and with the sequence t_p – τ – t_p – T – t_p – τ – echo, where during the time T, a radiofrequency (RF) pulse was applied. The interpulse delay τ was set to 1 µs, corresponding to the phase memory time T_m, where detection of small hyperfine couplings is most sensitive, and the RF pulse length to 50 µs.

Electron-electron double resonance (ELDOR)-detected NMR (EDNMR) spectra were acquired with an SRT of 1 ms and the echo-detected hole-burning sequence $t_{HTA} - T - t_p - \tau - 2t_p - \tau -$ echo, with t_{HTA}= 50 µs, T = 10 µs, t_p = 100 ns, τ = 1400 ns and an integration window of 1400 ns. The frequency of the high-turning angle (HTA) pulse was incremented in steps of 0.1 MHz over the measured range. A two-step phase cycle, +<x> - -<x>, on the π/2 pulse of the Hahn echo was used to eliminate unwanted coherence transfer pathways and cancel receiver offsets. The power of the HTA pulse, generated by the ELDOR channel of the spectrometer, was optimized such that the observed lines were as intense as possible without being broadened by saturation effects. The nutation frequency v_1 at the centre of the resonator was ca. 2 MHz or ca. 7 MHz, denoted as low and high HTA pulse power, respectively. The settings were held constant between peptide samples and the corresponding Mn-ATP control samples. Yet it is important to note that exact reproducibility of peak intensities between independent experiments may be difficult with the resonator used because the resonator profile strongly affects line intensities in EDNMR, and hence a careful experimental setup is required, particularly with respect to resonator bandwidth.

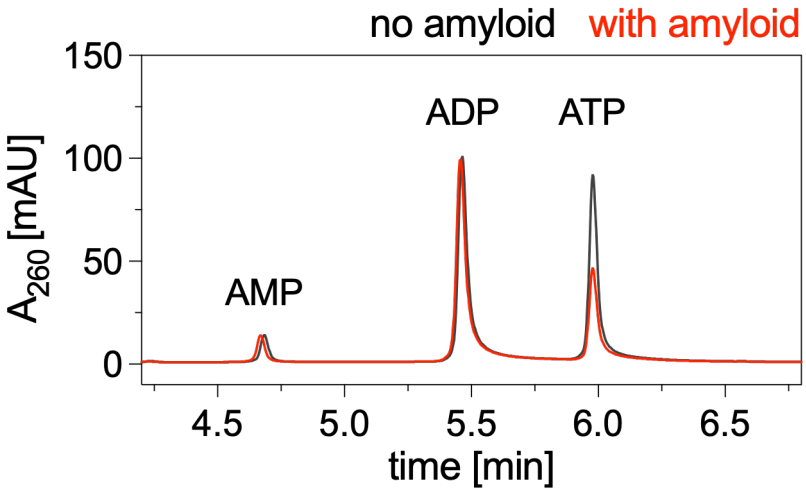


Figure S1. Short peptide amyloids selectively bind ATP over ADP. Representative reverse-phase HPLC analysis of ATP and ADP in the absence (black) and presence (red) of the peptide VFEFEFKFK, illustrating the preferential depletion of ATP relative to ADP. Experiments were conducted at room temperature in citrate–phosphate buffer (pH 3) using 100 µM peptide and 80 µM each of ATP and ADP. After 20 h of incubation, samples were centrifuged (25,000g, 1 h), and the supernatant was analyzed to quantify the fraction of unbound nucleotides remaining in solution. AMP, present as a minor contaminant in the ADP stock, does not bind to amyloids.

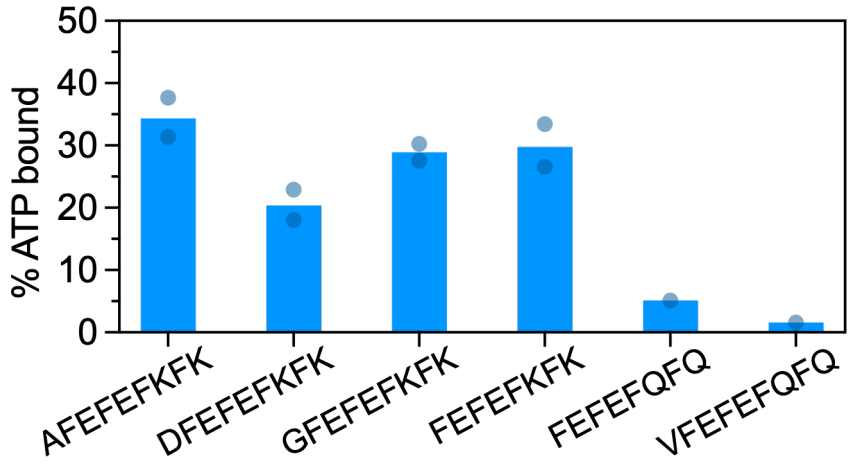


Figure S2. ATP binding to peptide amyloids of varying sequence and charge. The percentage of ATP bound to amyloids of different sequences and charge characteristics is shown. Experiments were performed at room temperature in citrate–phosphate buffer (pH 3) using 100 μM peptide and 80 μM ATP. After 20 h of incubation, samples were centrifuged (25,000g, 1 h), and the supernatant was analyzed by HPLC to determine the fraction of unbound ATP. The percentage of bound ATP was calculated by subtracting the unbound fraction from the total ATP concentration. Data represent the mean of two independent experiments (dots).

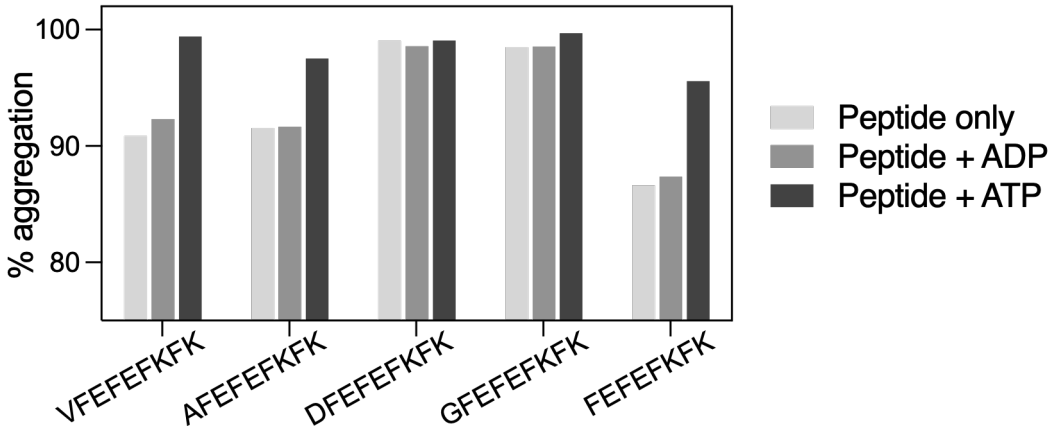


Figure S3. ATP promotes amyloid aggregation. The percentage of peptide aggregation for sequences with different charge characteristics in the presence of ATP or ADP is shown. Experiments were performed at room temperature in citrate–phosphate buffer (pH 3) using 100 μM peptide and 80 μM ATP or ADP. After 20 h of incubation, samples were centrifuged (25,000g, 1 h), and the supernatant was analyzed by HPLC to determine the soluble peptide fraction. The percentage of aggregated peptide was calculated from the decrease in soluble peptide relative to the total.

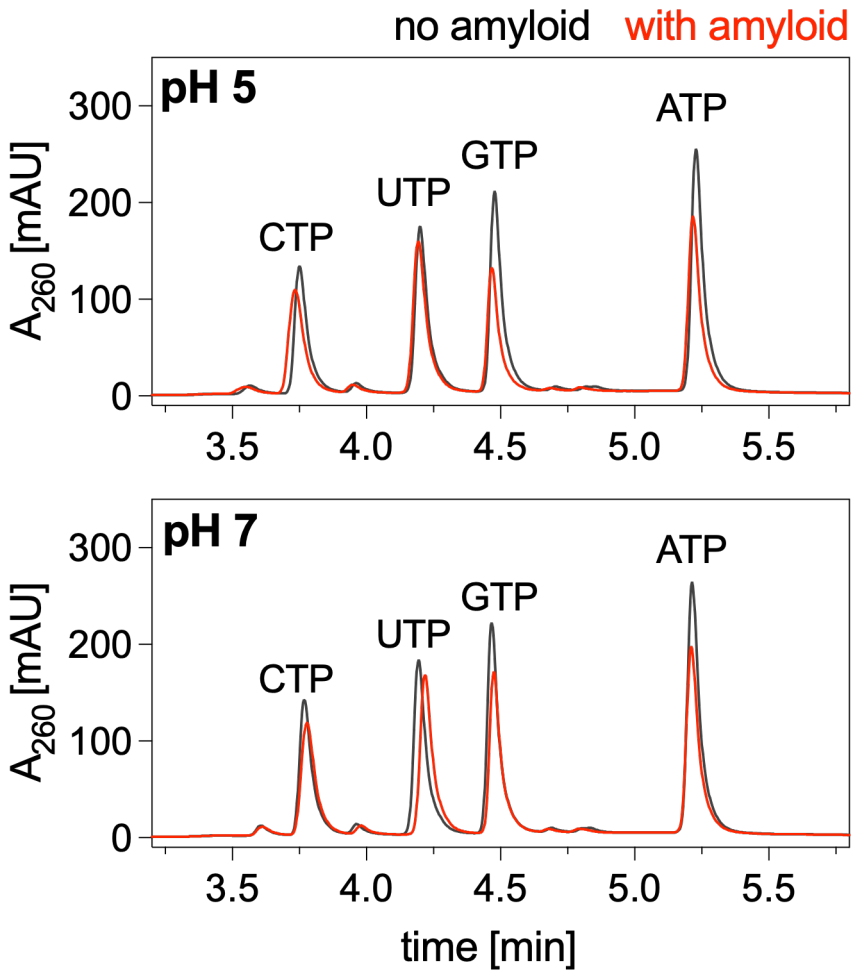


Figure S4. Reverse-phase HPLC chromatograms showing pH-dependent NTP binding to VAQAQINI-NH_2 amyloid. Representative HPLC traces of NTP (N = C, U, G, A) (black) and in the presence of amyloids (red) under competitive conditions at pH 5 and 7, illustrating selective nucleotide depletion, with reduced binding observed at higher pH. Experiments were performed at room temperature in citrate–phosphate buffer (pH 5) or phosphate buffer (pH 7) using 1 mM peptide and 250 µM of each nucleoside triphosphate. After incubation, samples were centrifuged (25,000g, 1 h), and nucleotide concentrations in the supernatant were determined by analytical reverse-phase HPLC.

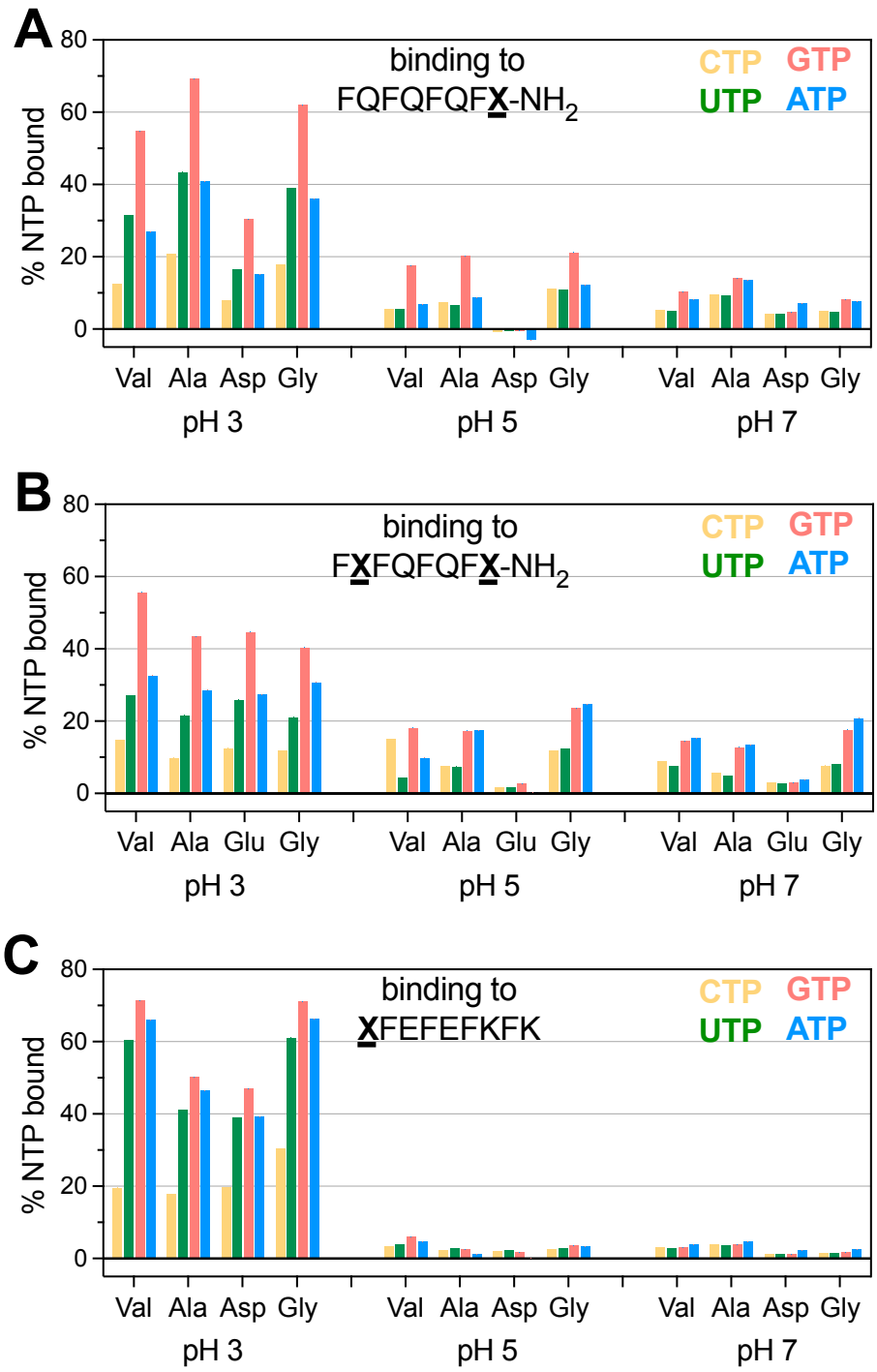


Figure S5. pH-dependent selective binding of NTPs by peptide amyloids. Binding of CTP, UTP, GTP, and ATP (color-coded) was quantified for amyloids formed by **(A)** FQFQFQFX-NH_2, **(B)** FXFQFQFX-NH_2, and **(C)** XFEFEFKFK peptides (X = Val, Ala, Asp/Glu, Gly) under competitive conditions at pH 3, 5, and 7. Overall nucleotide association is enhanced at acidic pH, whereas binding decreases at higher pH, consistent with reduced protonation of ionizable groups and weakened electrostatic interactions with the triphosphate moiety. Experiments were performed at room temperature in citrate–phosphate buffer (pH 3 and 5) or phosphate buffer (pH 7) using 1 mM peptide and 250 μM of each nucleoside triphosphate. Nucleotide concentrations were determined by analytical reverse-phase HPLC.

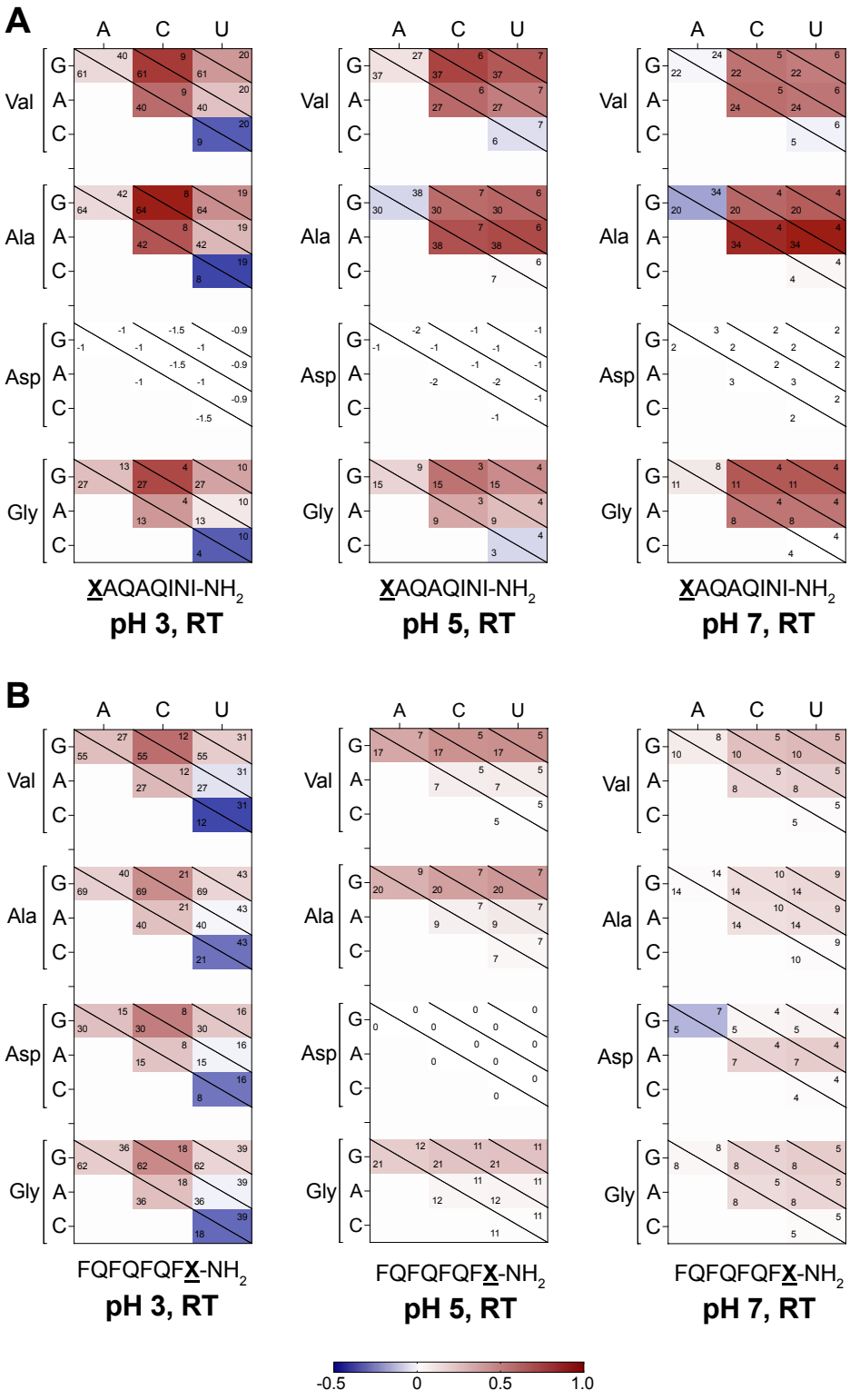


Figure S6. Pairwise selectivity of NTP binding to peptide amyloids (continued below).

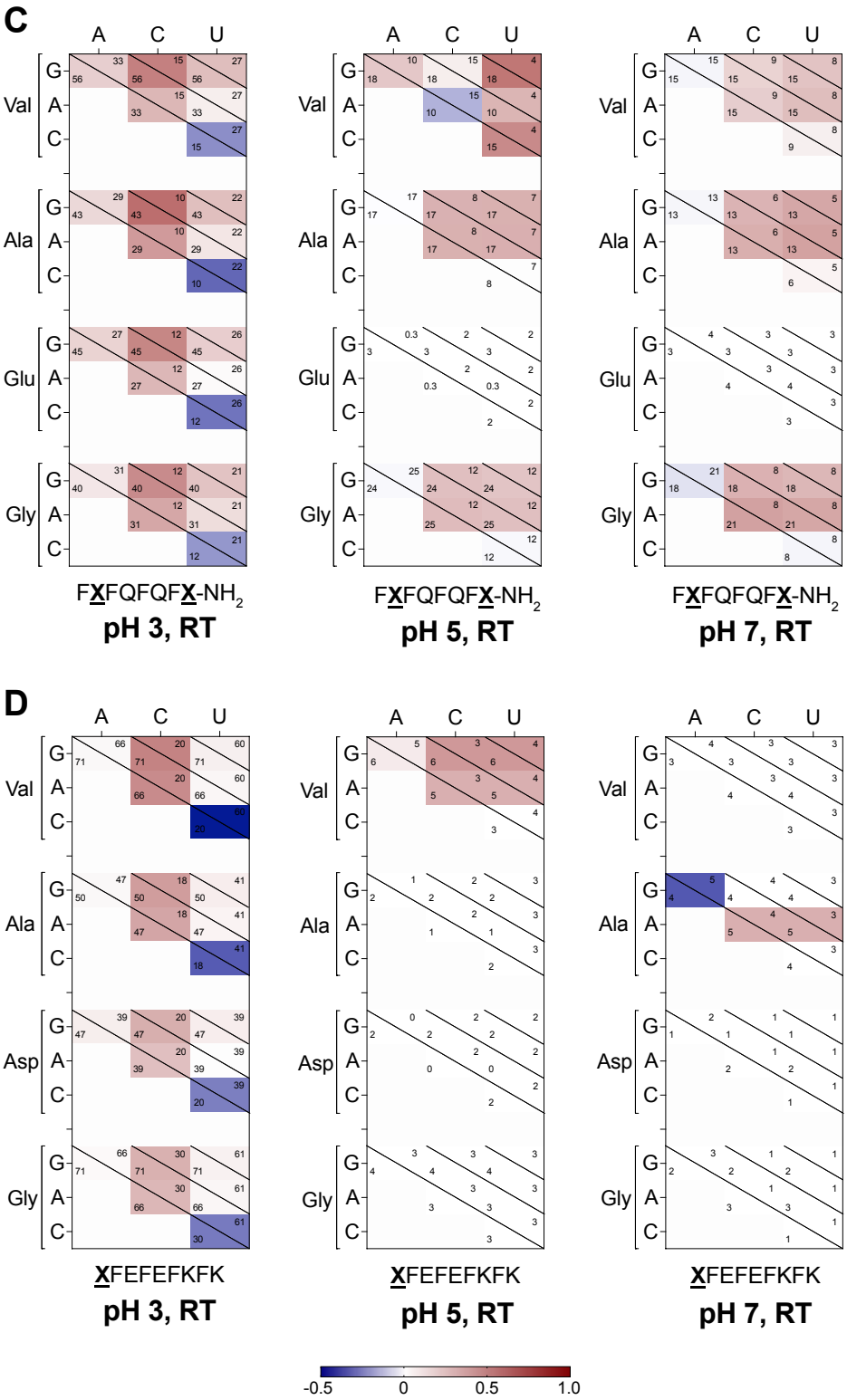


Figure S6. Pairwise selectivity of NTP binding to peptide amyloids. Heatmaps showing the logarithm of the ratio of percentage bound nucleoside triphosphates for all pairwise nucleotide combinations, visualizing relative binding preferences for individual peptide amyloids. Data are shown for representative peptide sets: **(A)** XAQAQINI-NH_2, **(B)** FQFQFQFX-NH_2, **(C)** FXFQFQFX-NH_2, and **(D)** XFEFEFKFK peptides (X = Val, Ala, Asp/Glu, Gly). Positive (red) and negative (blue) values indicate preferential binding of one nucleotide over another, while values near zero indicate similar binding. Absolute percentage binding values for each nucleotide are indicated within the plots. Pairwise ratios were not calculated

when either nucleotide showed <4% absolute binding; these comparisons are shown without color. Peptide and nucleotide concentrations, as well as pH conditions, are specified in each panel and correspond to the experimental conditions described in **Figure S5**. Percentage binding values were calculated from analytical reverse-phase HPLC measurements of nucleotide depletion from the supernatant.

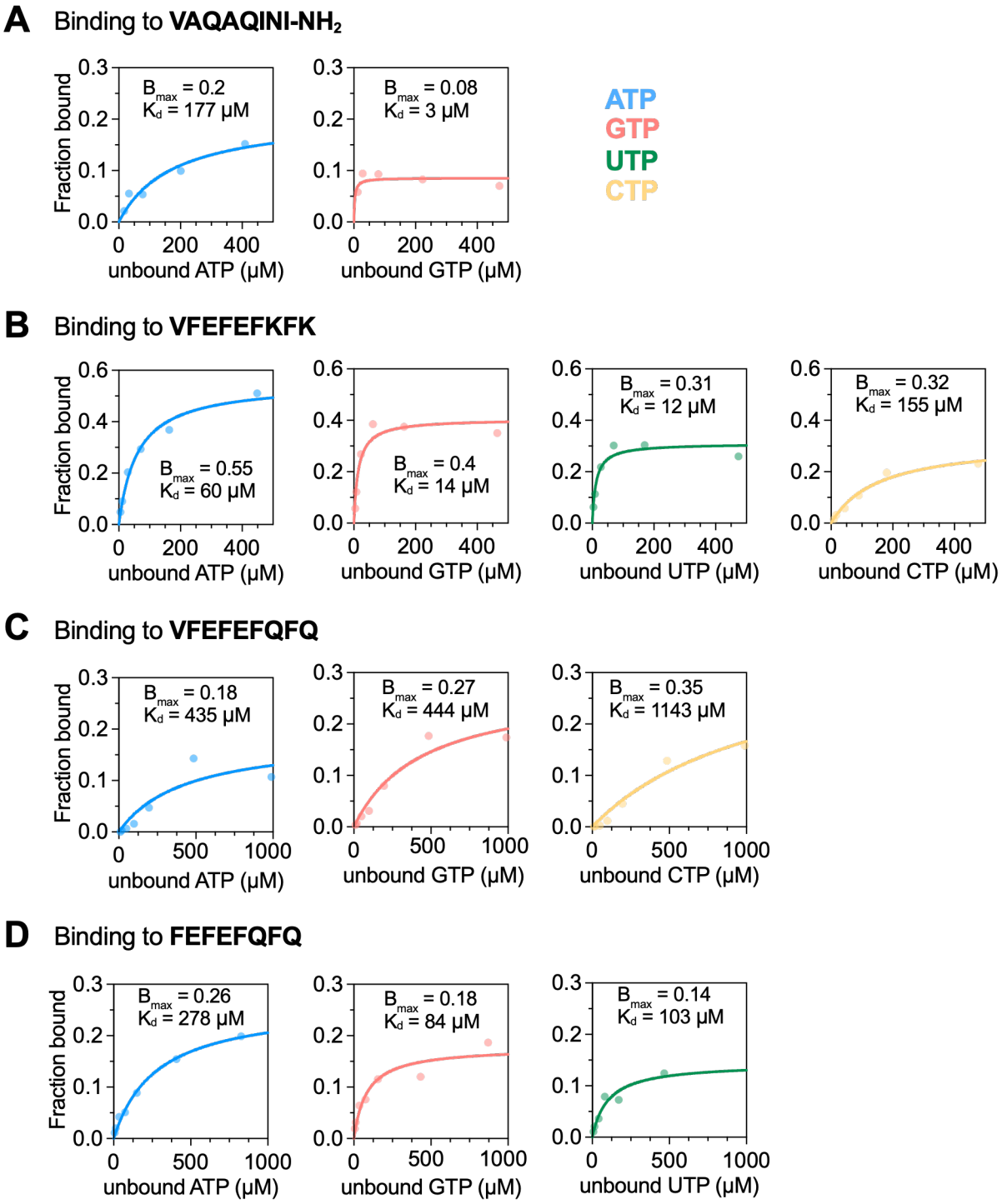


Figure S7. Binding affinities of NTP–amyloid interactions. Binding dissociation constants (K_d) for interactions between NTP (ATP, GTP, UTP, and CTP) and peptide amyloids: **(A)** VAQAQINI-NH_2, **(B)** VFEFEFKFK, **(C)** VFEFEFQFQ, **(D)** FEFEFQFQ. HPLC analyses of the supernatant from mixtures of 100 μM peptide and 10-1000 μM NTP at pH 3 (citrate-phosphate

buffer) were performed to obtain the fraction bound (ratio of NTP to peptide in the pellet) as a function of unbound NTP. The data were fit to a model for a single binding site to yield the K_d and maximum fraction bound. Curve fitting and data analysis were performed using GraphPad Prism (version 11.0.0).

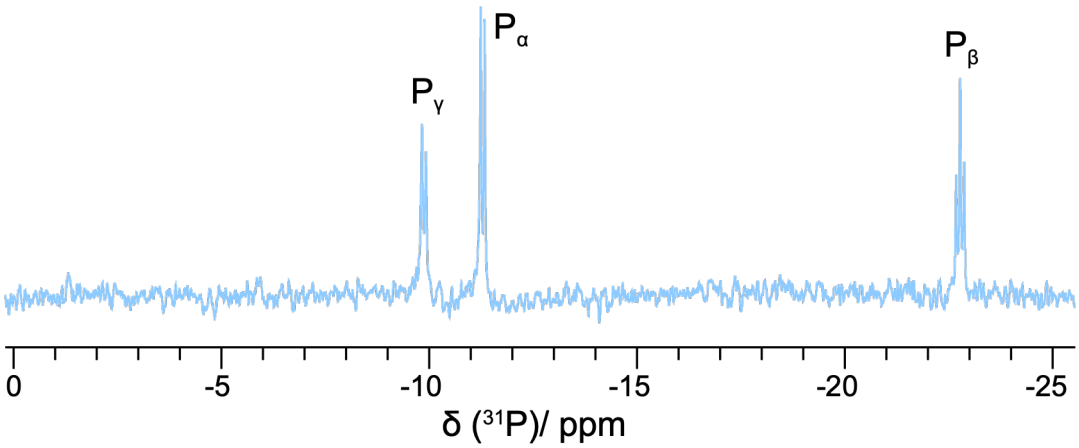


Figure S8. Reference solution-state ^{31}P NMR spectrum of ATP. The spectrum was recorded for 1 mM ATP in acetate buffer at pH 6, showing the characteristic P_β triplet at approximately −23 ppm and the P_α and P_γ doublets. The spectrum was acquired on a Bruker Avance NEO 500 MHz spectrometer (^{31}P resonance frequency, 202.4 MHz).

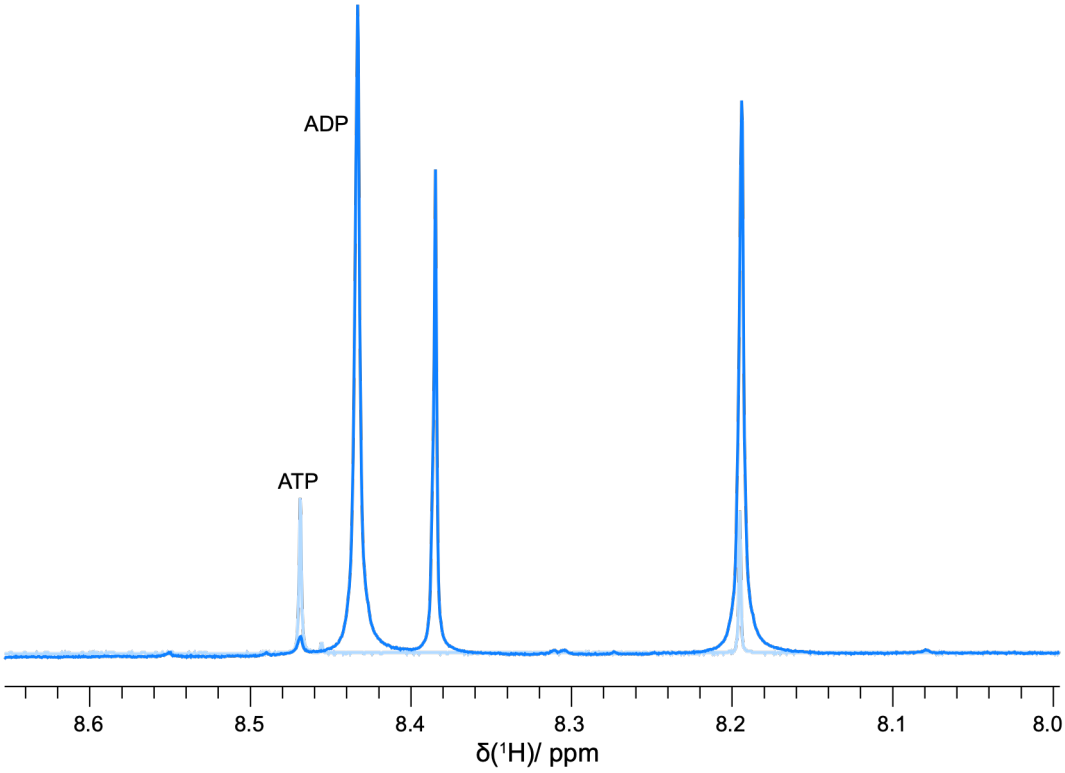


Figure S9. ^{1}H NMR confirmation of ATP formation in the reaction of ADP and acetyl phosphate mediated by peptide amyloids in the presence of $MgCl_2$. Representative aromatic region of the ^{1}H NMR spectra of the reaction mixture overlaid with an authentic ATP reference spectrum (light blue). The reaction spectrum exhibits resonances consistent with ATP, including the characteristic adenine proton signals that are distinguishable from those of

ADP, providing independent support for ATP formation observed by reverse-phase HPLC and ^{31}P NMR. Spectra were acquired on a Bruker AV IIIHD 900 MHz spectrometer.

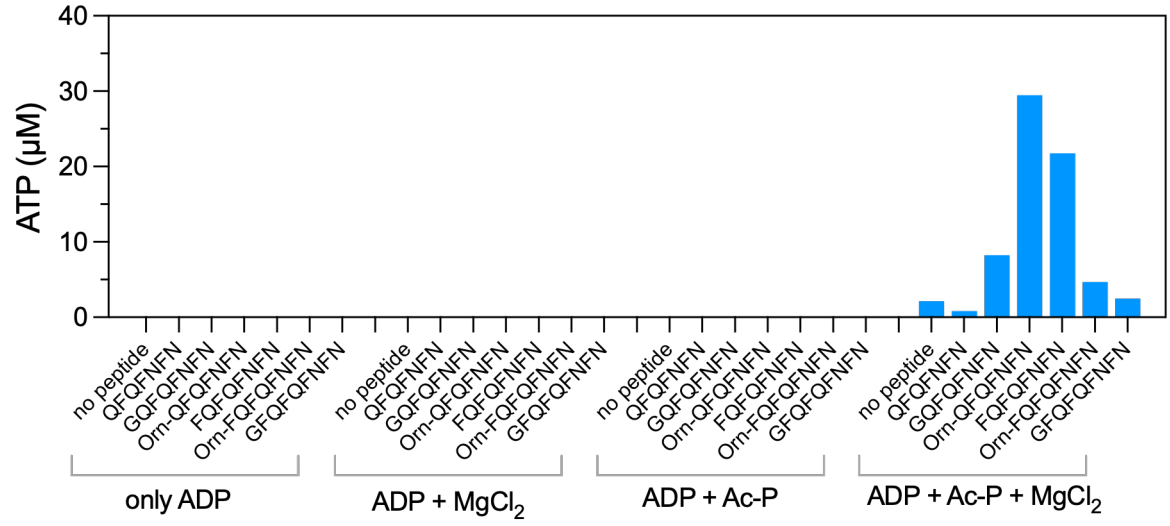


Figure S10. ATP formation from ADP and acetyl phosphate mediated by peptide amyloids. ATP formation was quantified by reverse-phase HPLC at pH 5 in the absence and presence of 20 mM $MgCl_2$ for amyloidogenic peptides (as indicated in the figure; Orn = ornithine) differing in the number of positive charges (one at the N-terminus or two at the N-terminus and Orn) and possessing a free C-terminus. ATP formation was not detected in the absence of Mg^{2+}, whereas the addition of Mg^{2+} promoted activity for the sequences. Experiments were performed at room temperature in 40 mM sodium acetate buffer (pH 5) using 1 mM peptide amyloid, 1.2 mM ADP, and 5 mM acetyl phosphate for 20 h.

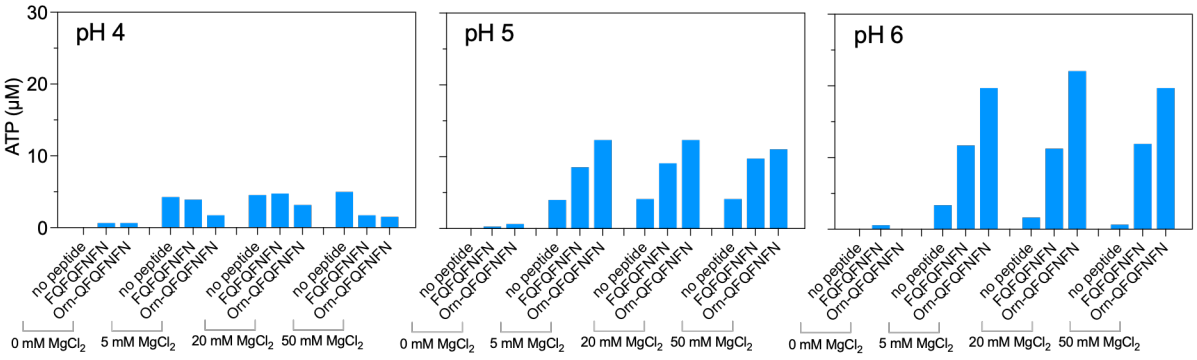


Figure S11. pH- and Mg^{2+} concentration-dependent ATP formation from ADP and acetyl phosphate by peptide amyloids. ATP formation was quantified by reverse-phase HPLC at pH 4, 5 and 6 in the absence and presence of 5-50 mM $MgCl_2$ for amyloidogenic peptides (as indicated in the figure; Orn = ornithine) differing in the number of positive charges (one at the N-terminus or two at the N-terminus and Orn) and possessing a free C-terminus. ATP formation was negligible in the absence of Mg^{2+}, whereas the addition of Mg^{2+} enhanced activity for the peptides. ATP formation displayed a clear pH dependence, with higher activity at pH 6. At higher Mg^{2+} concentrations (50 mM), a slight decrease in activity was observed relative to lower Mg^{2+} concentrations. Experiments were performed at room temperature in 40 mM acetate buffer (pH 4–6) using 1 mM peptide amyloid, 1.2 mM ADP, and 5 mM acetyl phosphate for 20 h.

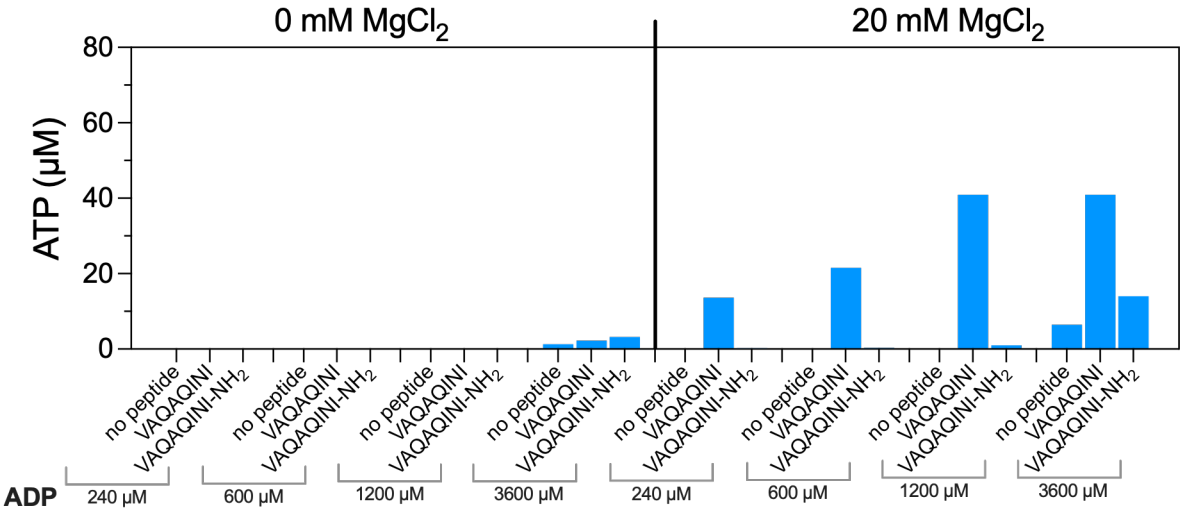


Figure S12. ATP formation by peptide amyloids as a function of ADP concentration. ATP formation was quantified by reverse-phase HPLC at pH 7 in 40 mM sodium phosphate buffer in the absence and presence of 20 mM $MgCl_2$ for amyloidogenic peptides (1 mM) bearing a single N-terminal positive charge and either a free or amidated C-terminus (VAQAQINI and VAQAQINI-NH_2). Reactions were performed with varying ADP concentrations (240 μM–3.6 mM) and 5 mM acetyl phosphate. ATP formation was negligible in the absence of Mg^{2+}, whereas the addition of Mg^{2+} promoted ATP formation for both peptides, with yields increasing at higher ADP concentrations. Experiments were performed at room temperature for 20 h.

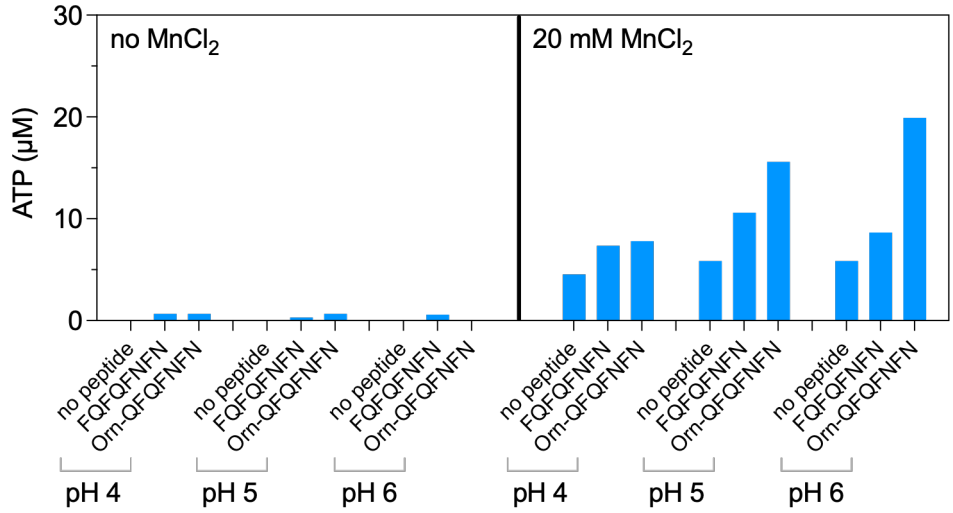


Figure S13. pH- and Mn^{2+}-dependent ATP formation from ADP and acetyl phosphate mediated by peptide amyloids. ATP formation was quantified by reverse-phase HPLC at pH 4, 5, and 6 in the absence and presence of 20 mM $MnCl_2$ for amyloidogenic peptides (as indicated in the figure; Orn = ornithine) differing in the number of positive charges (one at the N-terminus or two at the N-terminus and Orn) and possessing a free C-terminus. ATP formation was negligible without Mn^{2+}, but increased with Mn^{2+}, showing higher activity at pH 6. Experiments were performed at room temperature in 40 mM acetate buffer (pH 4–6) using 1 mM peptide amyloid, 1.2 mM ADP, and 5 mM acetyl phosphate for 20 h.

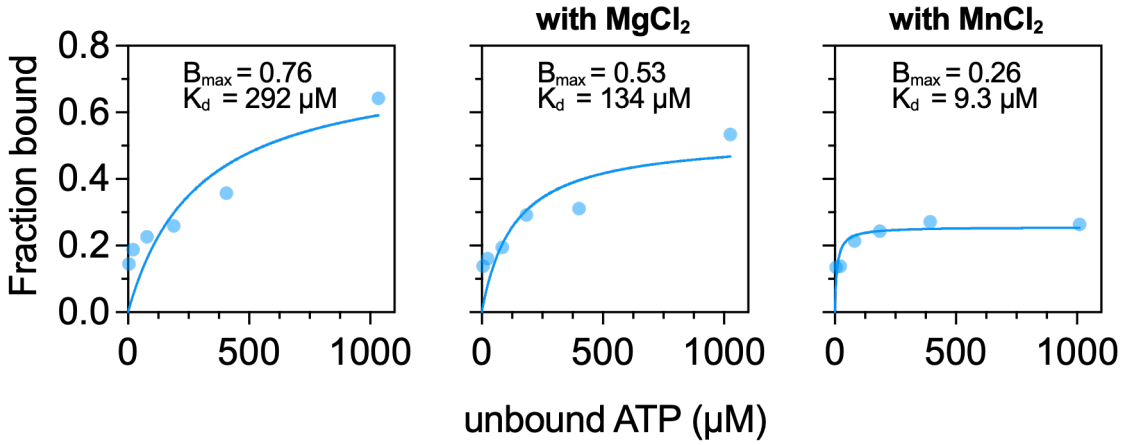


Figure S14. Binding affinities of ATP–amyloid interactions in the presence of divalent metal ions. Dissociation constants (K_d) for the interaction between ATP and VAQAQINI-NH_2 were determined in the presence of 2 mM Mg^{2+} or Mn^{2+} at pH 4 (40 mM acetate buffer). HPLC analysis of supernatants from mixtures containing 100 µM peptide and 10–1000 µM ATP was used to calculate the fraction bound (ratio ATP to peptide in the pellet) as a function of unbound ATP. The resulting data were fit using a single-site binding model to extract K_d values and maximum binding fractions. Curve fitting and analysis were carried out with GraphPad Prism (version 11.0.0).

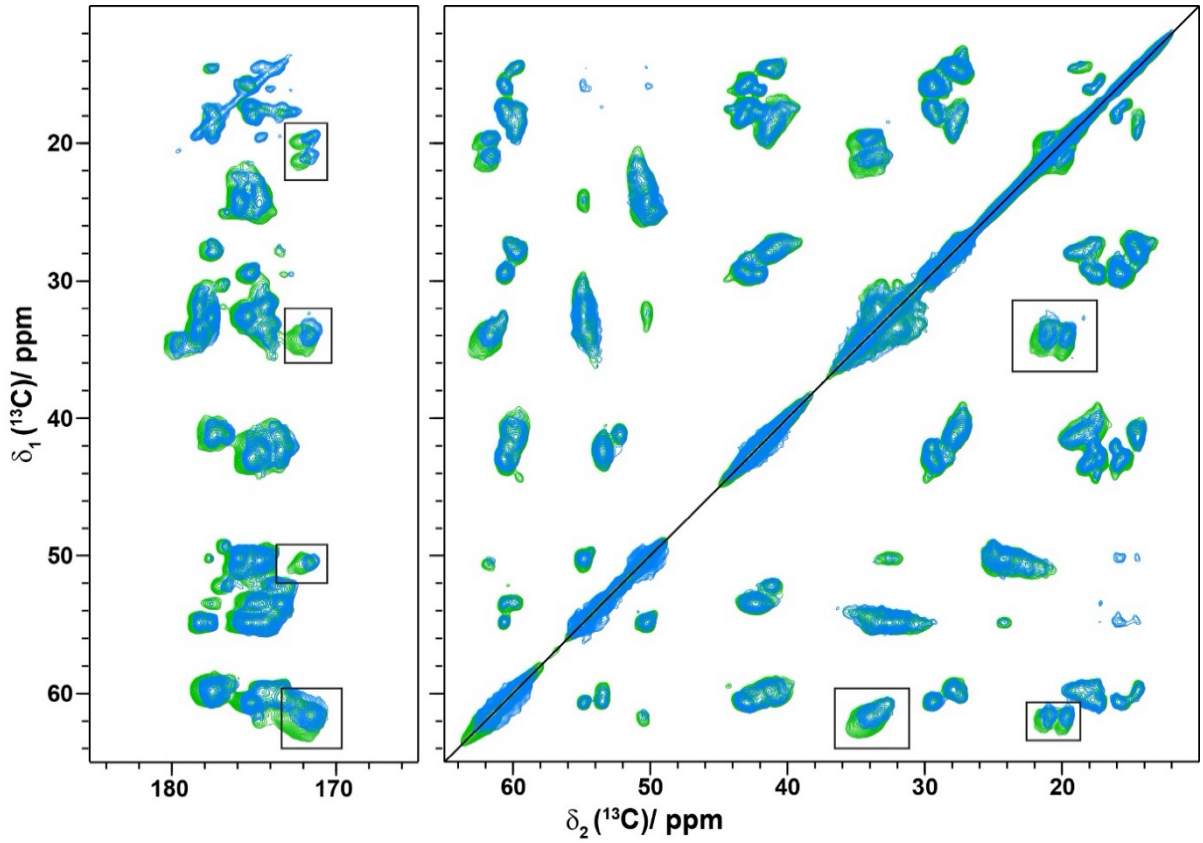


Figure S15. ^{13}C-^{13}C DARR spectra reveal chemical-shift perturbations upon ATP binding. 2D ^{13}C-^{13}C DARR spectra of uniformly $^{13}C/^{15}N$ labelled VAQAQINI-NH_2 (blue), which was published previously by Rout et al.[3] and uniformly $^{13}C/^{15}N$ labelled VAQAQINI-NH_2:ATP

(green), recorded with a mixing time of 20 ms. Clearly visible chemical-shift perturbations are observed for Val1 and the corresponding resonances are marked by black rectangles. The spectrum of VAQAQINI-NH_2 was recorded at a static magnetic-field strength of 20.0 T, while the spectrum of VAQAQINI-NH_2:ATP was recorded at a static magnetic field strength of 16.4 T. Both spectra were recorded with an MAS frequency of 17.0 kHz. The peptide is C-terminally amidated.

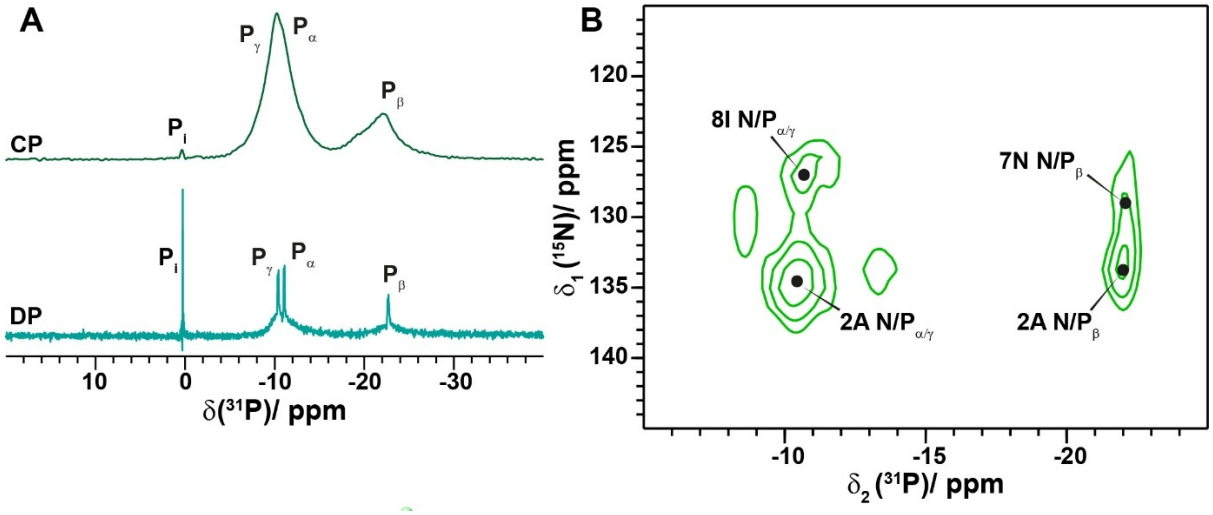


Figure S16. Interactions between amyloid and ATP were confirmed from a ^{15}N-^{31}P NHHP correlation experiment. (**A**) ^{1}H-^{31}P CP-MAS NMR spectrum (green) and ^{31}P DP spectrum (turquoise) of uniformly ^{13}C/^{15}N labelled VAQAQINI-NH_2:ATP. Both spectra were normalized to the most intense resonance. (**B**) 2D ^{15}N-^{31}P NHHP spectrum (200 µs ^{1}H-^{1}H spin-diffusion time) of uniformly ^{13}C/^{15}N labelled VAQAQINI-NH_2:ATP, which probes peptide–nucleotide spatial proximities. All spectra were recorded at a static magnetic-field strength of 11.7 T using an MAS frequency of 17.0 kHz. The peptide is C-terminally amidated.

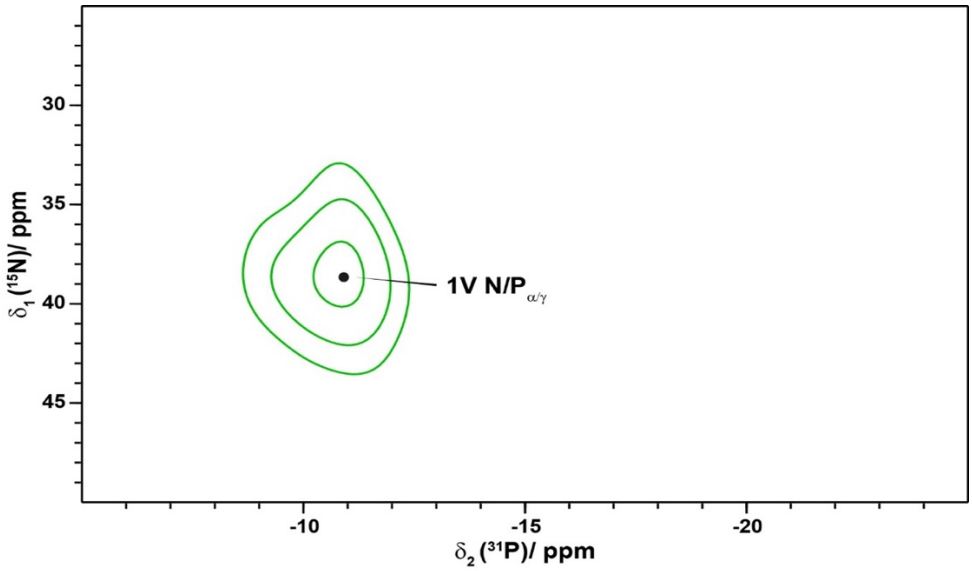


Figure S17. The ^{15}N-^{31}P NHHP spectrum of the N-terminal region of VAQAQINI-NH_2:ATP shows spatial proximity between the N-terminus and ATP. 2D ^{15}N-^{31}P NHHP spectrum

(200 µs ^{1}H-^{1}H spin-diffusion time) focusing on the low-frequency ^{15}N region of uniformly ^{13}C/^{15}N labelled VAQAQINI-NH_2:ATP recorded at a static magnetic-field strength of 11.7 T using an MAS frequency of 17.0 kHz. The peptide is C-terminally amidated.

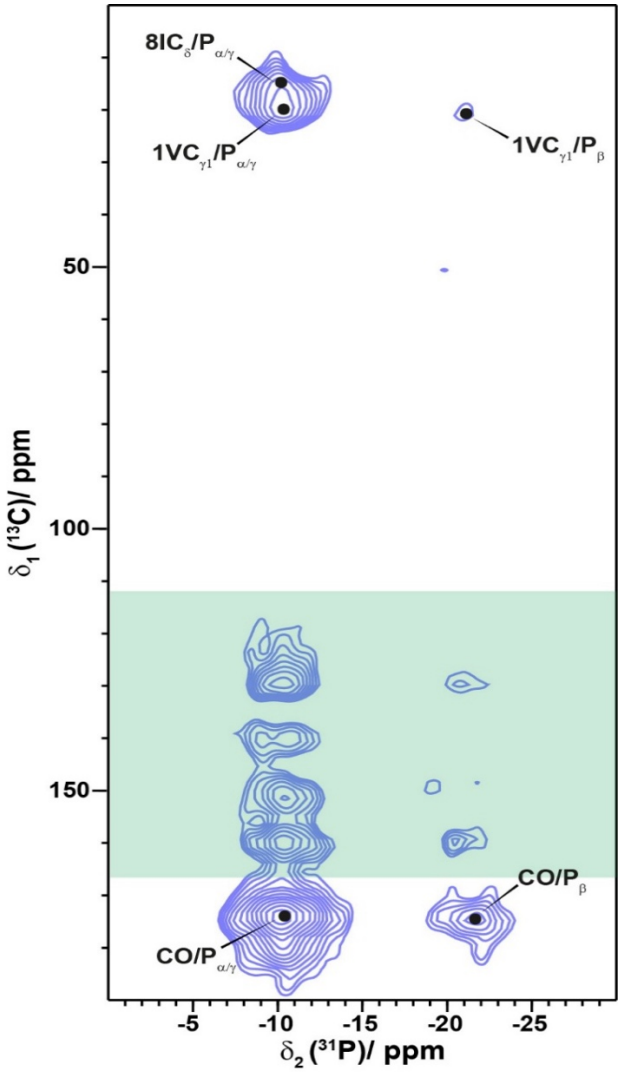


Figure S18. The ^{13}C-^{31}P CHHP spectrum shows spatial proximity between residues Val1 and Ile8 of VAQAQINI-NH_2 and the phosphates of ATP. 2D ^{13}C-^{31}P CHHP spectrum (200 µs ^{1}H-^{1}H spin-diffusion time) of uniformly ^{13}C/^{15}N labelled VAQAQINI-NH_2:ATP recorded at a static magnetic-field strength of 11.7 T using an MAS frequency of 17.0 kHz. Marked with a green square are spectral artifacts whose origin remains unclear. The peptide is C-terminally amidated.

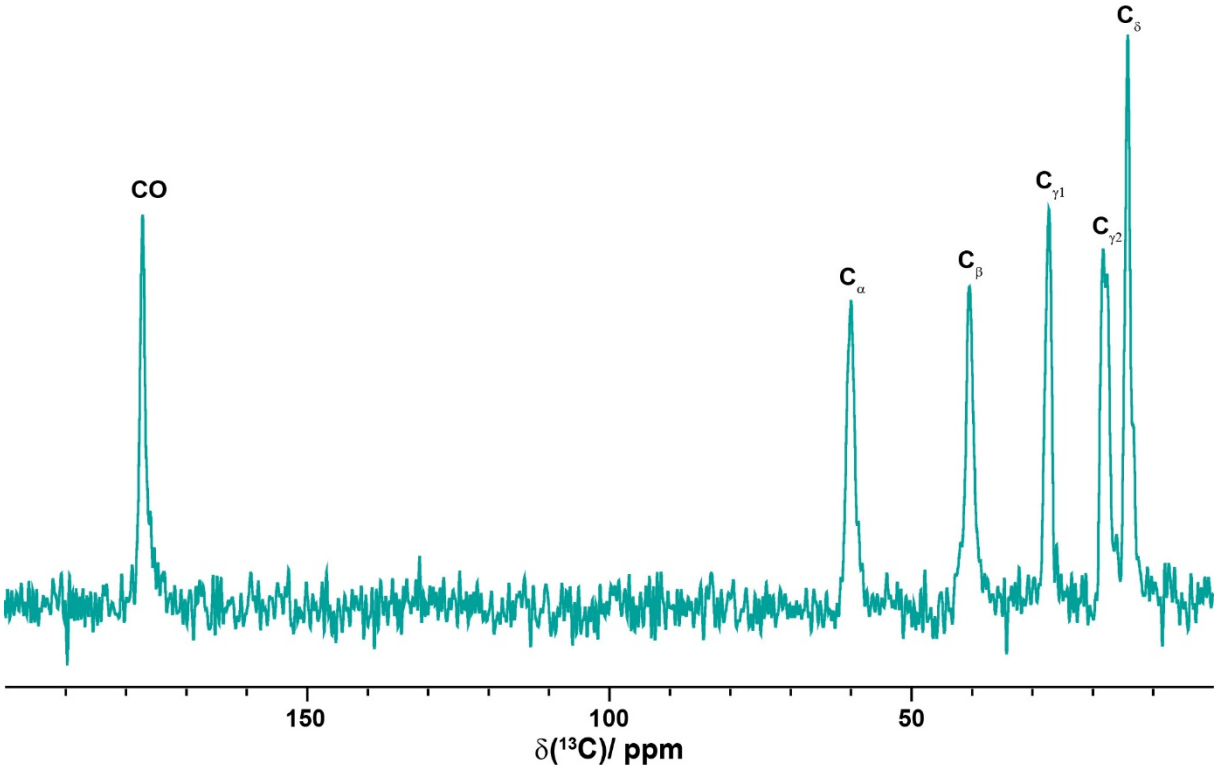


Figure S19. The ordered amyloid state is preserved after incubation with ADP and acetyl phosphate. ^{1}H-^{13}C CP MAS spectrum of VAQAQIN(^{13}C)I-NH_2:ADP:AcP recorded at a static magnetic-field strength of 11.7 T using an MAS frequency of 17.0 kHz. The peptide is C-terminally amidated.

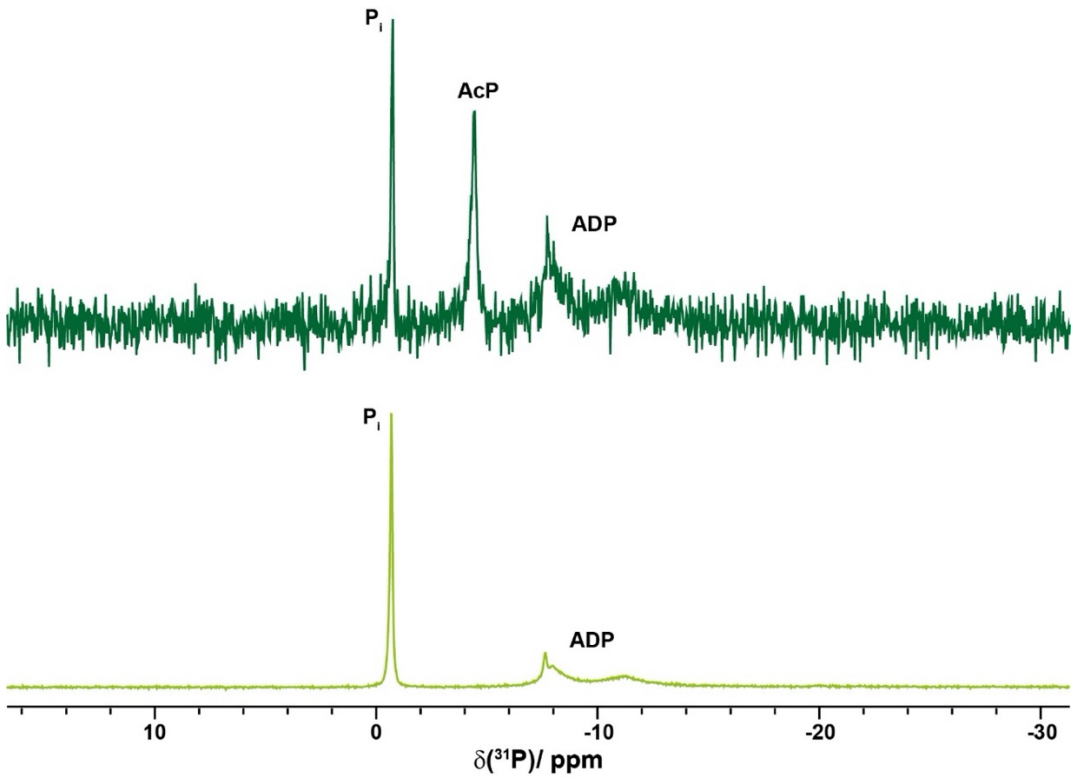


Figure S20. The ADP–AcP mixture is not sufficiently stable over multiple days for solid-state NMR measurements. ^{31}P DP spectrum of VAQAQIN(^{13}C)I-NH_2:ADP:AcP measured directly after sample preparation (dark green) and five days after sample preparation (light green). Both spectra were recorded at a static magnetic-field strength of 11.7 T using an MAS frequency of 17.0 kHz.

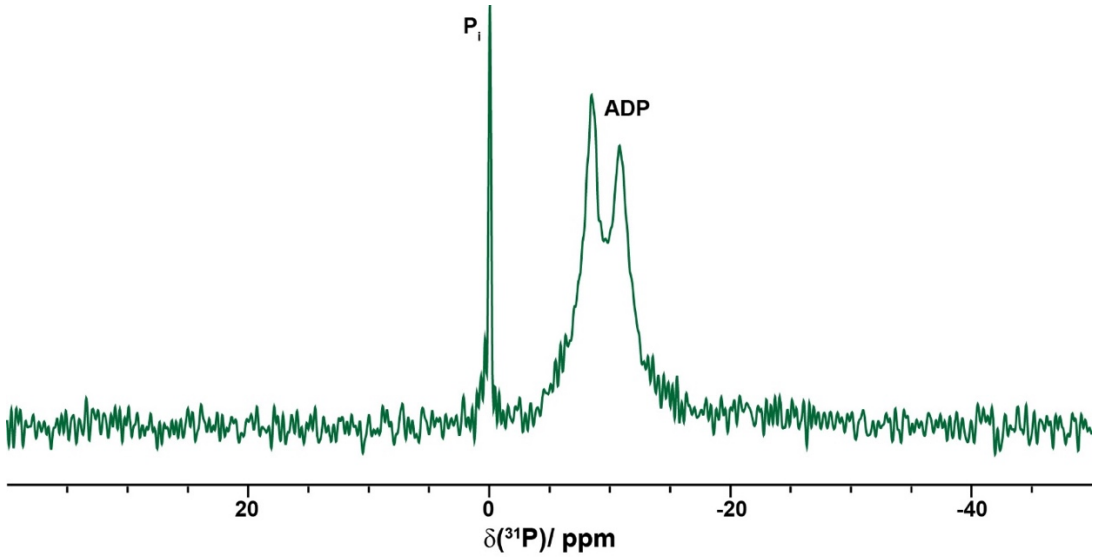


Figure S21. Excess ADP remains undissolved under the reaction conditions. ^{1}H-^{31}P CP-MAS spectrum of the VAQAQIN(^{13}C)I-NH_2:ADP:AcP sample prepared with a large excess of ADP and acetyl phosphate (AcP). The observed ADP signals arise from solid-phase ADP. The spectrum was recorded at a static magnetic-field strength of 11.7 T using an MAS frequency of 17.0 kHz.

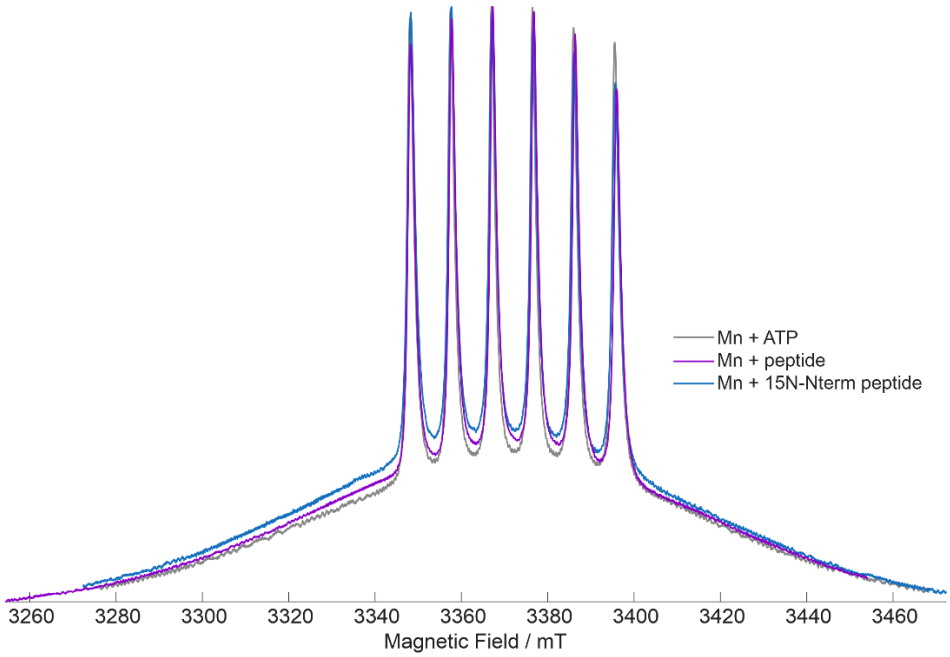


Figure S22. W-band echo-detected EPR spectra using peptides VAQAQINI-NH_2 and (^{15}N)VAQAQIN(^{13}C)I-NH_2 with 12 / 24 ns π/2 / π pulses and τ = 400 ns; further pulse EPR experiments were carried out on the third Mn line.

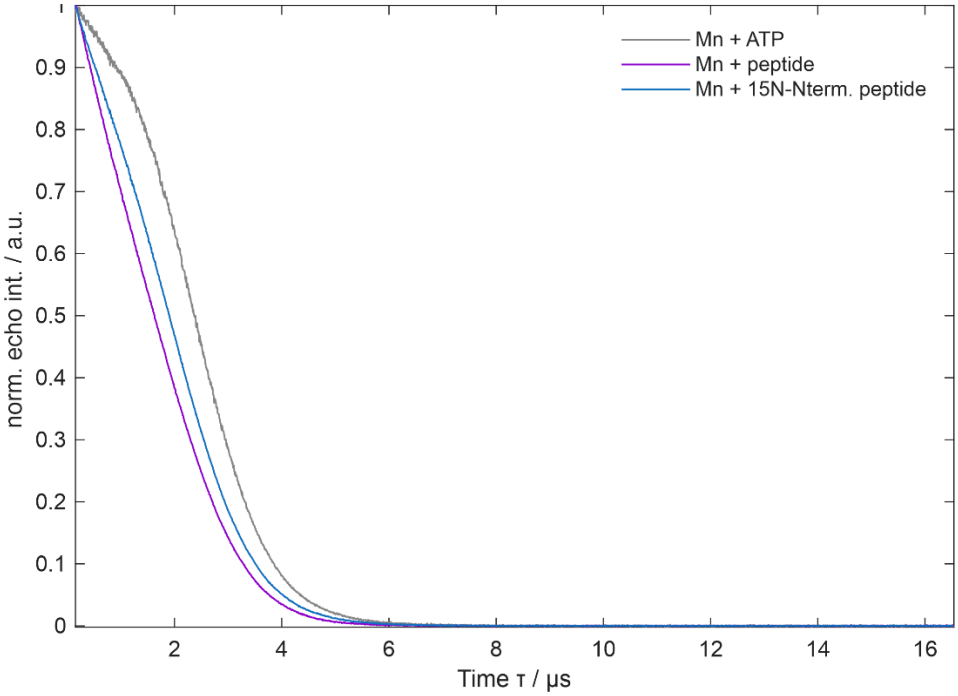


Figure S23. W-band 2pESEEM using peptides VAQAQINI-NH_2 and (^{15}N)VAQAQIN(^{13}C)I-NH_2 based on a Hahn echo sequence with 12 / 24 ns π/2 / π pulses.

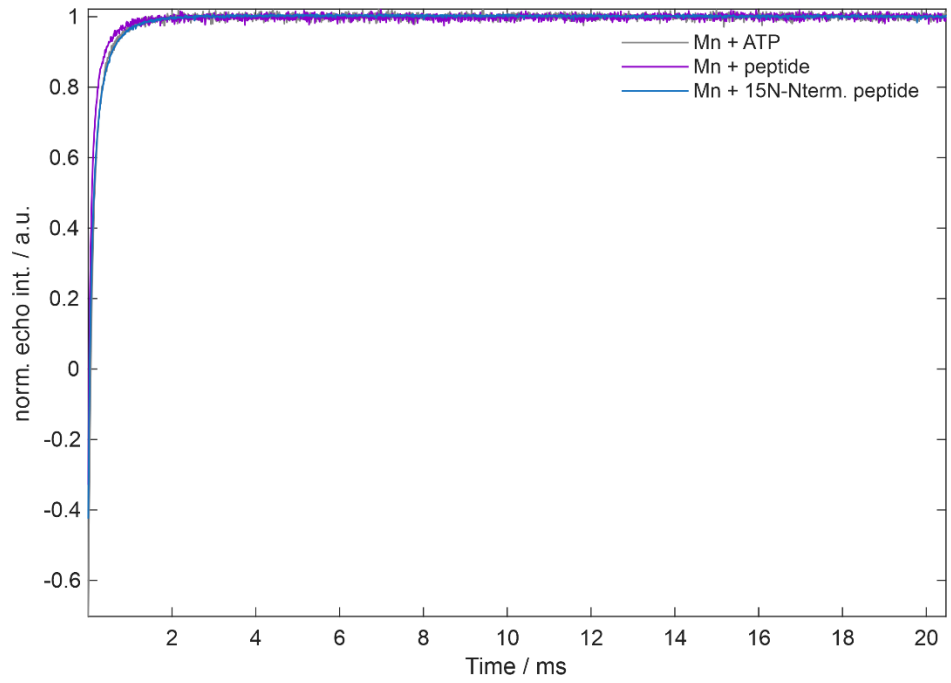


Figure S24. W-band T_1 relaxation measured by inversion recovery using peptides VAQAQINI-NH_2 and (^{15}N)VAQAQIN(^{13}C)I-NH_2 with a 24 ns inversion pulse and 12 / 24 ns π/2 / π pulses.

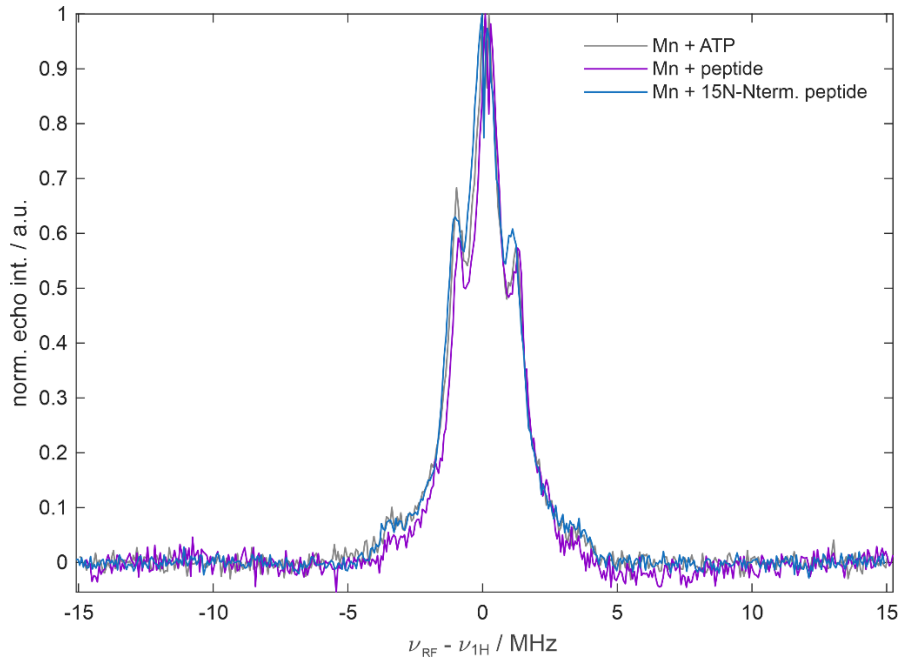


Figure S25. W-band ^{1}H Davies ENDOR using peptides VAQAQINI-NH_2 and (^{15}N)VAQAQIN(^{13}C)I-NH_2 showing similar ^{1}H hyperfine couplings (slight center shift, likely due to a residual magnetic field offset).

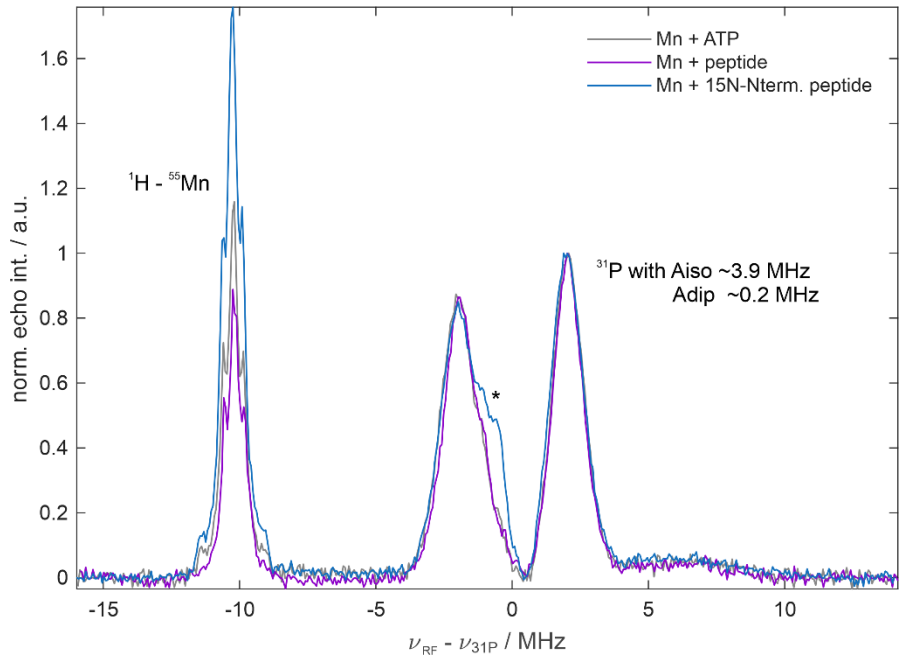


Figure S26. W-band ^{31}P Davies ENDOR using peptides VAQAQINI-NH_2 and (^{15}N)VAQAQIN(^{13}C)I-NH_2 showing ^{31}P hyperfine couplings. The inner shoulder (*), present in all samples with varying intensity, is more pronounced in the ^{15}N N-terminally labeled peptide sample.

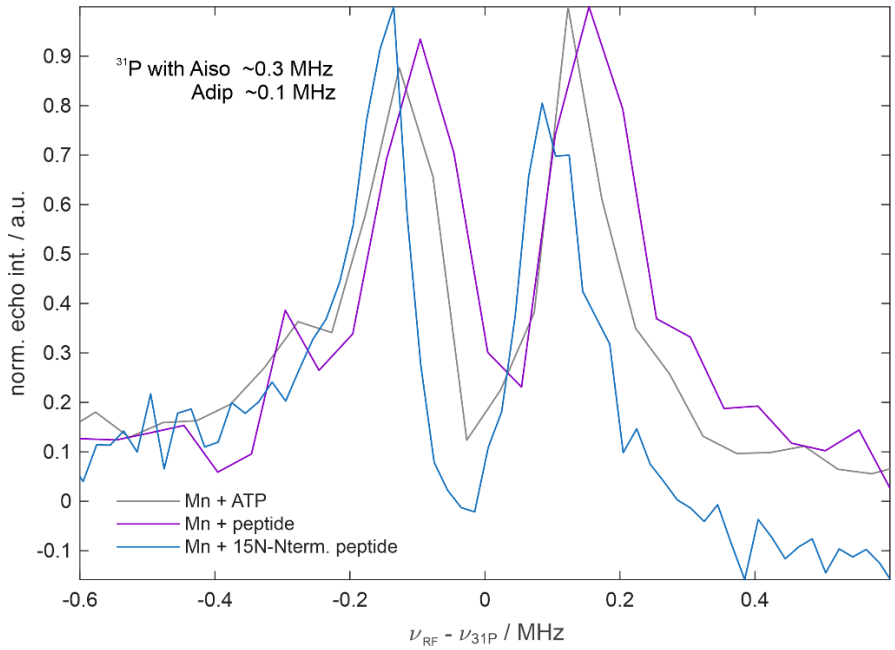


Figure S27. W-band ^{31}P Mims ENDOR (sensitive to small hyperfine couplings) using peptides VAQAQINI-NH_2 and (^{15}N)VAQAQIN(^{13}C)I-NH_2 showing the presence of at least one weakly coupled ^{31}P doublet (slight center shift, likely due to a residual magnetic field offset). The small ENDOR effect achieved allows only a limited signal-to-noise ratio in spite of a long acquisition time.

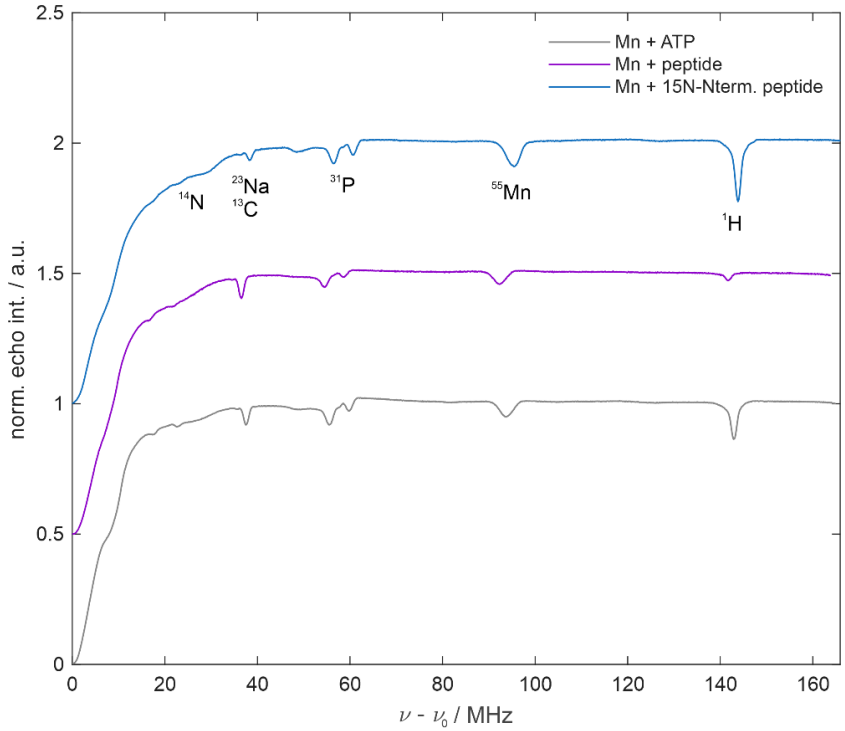


Figure S28. W-band EDNMR spectra using high power for the high turning angle pulse to increase sensitivity in a trade-off with increased broadening using peptides VAQAQINI-NH_2 and (^{15}N)VAQAQIN(^{13}C)I-NH_2.

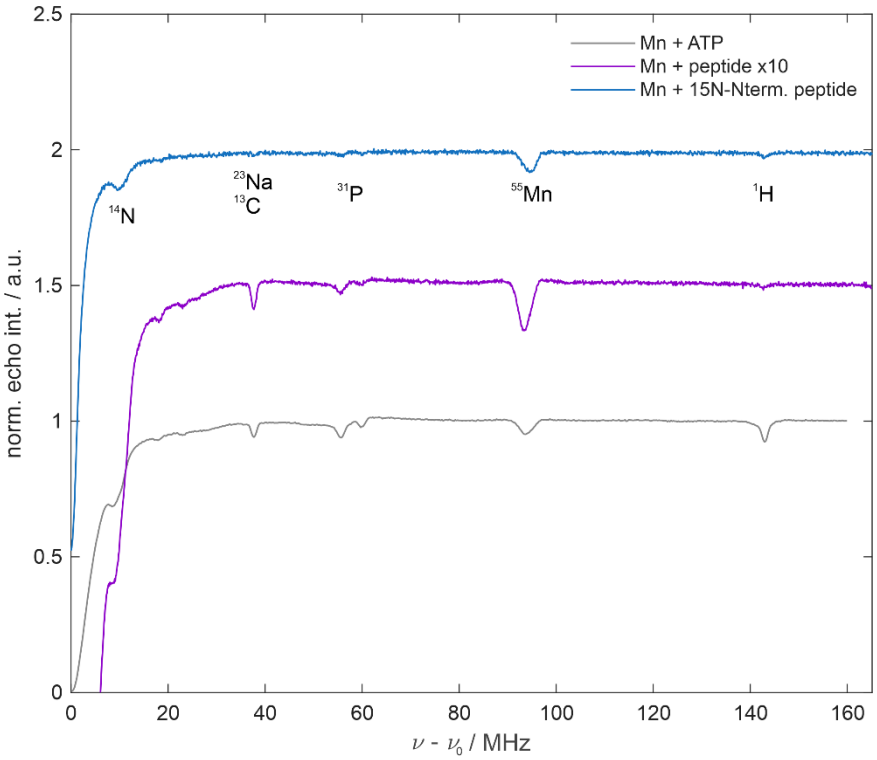


Figure S29. W-band EDNMR spectra using low power for the high turning angle pulse to increase resolution in a trade-off with sensitivity using peptides VAQAQINI-NH_2 and (^{15}N)VAQAQIN(^{13}C)I-NH_2.

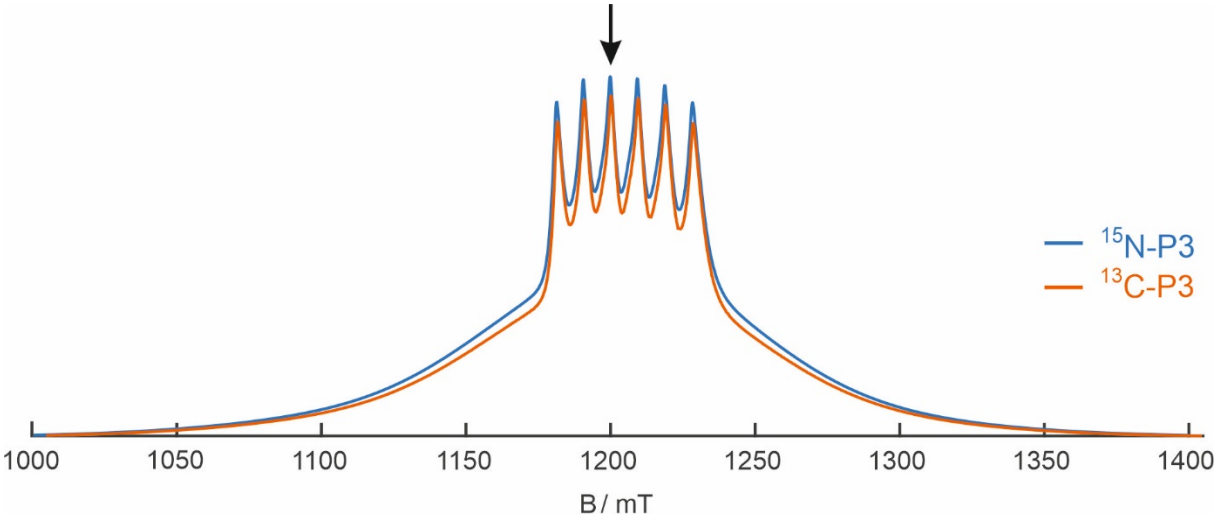


Figure S30. Q-band echo-detected EPR spectra recorded with 16 / 32 ns π/2 / π pulses and τ = 400 ns; the field position for pulse EPR experiments is indicated with an arrow. The peptides used were (^{15}N)VAQAQIN(^{13}C)I-NH_2 and (^{13}C)VAQAQIN(^{15}N)I-NH_2 denoted by ^{15}N-P3 and ^{13}C-P3. For comparison, the magnetic field axis of the ^{15}N-P3 spectrum was rescaled from 33.7 to 33.77 GHz. The black arrow marks the magnetic field position of further pulse EPR experiments.

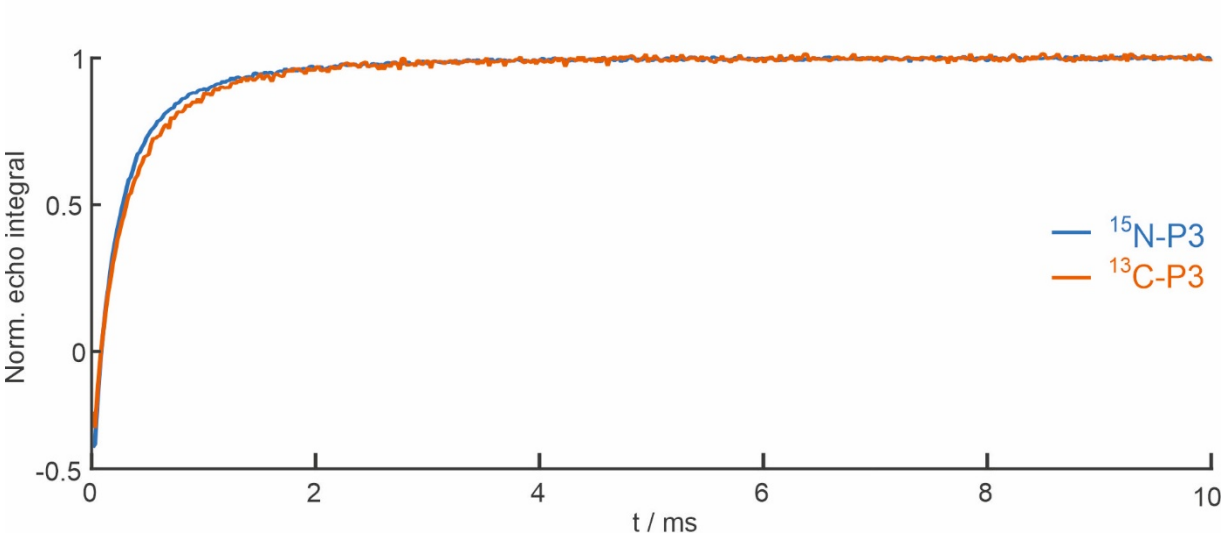


Figure S31. Q-band inversion recovery experiment using a 6.4 ns π inversion pulse and an SRT of 25 ms showing similar T_1 relaxation for the two peptide samples (^{15}N)VAQAQIN(^{13}C)I-NH_2 and (^{13}C)VAQAQIN(^{15}N)I-NH_2, denoted by ^{15}N-P3 and ^{13}C-P3.

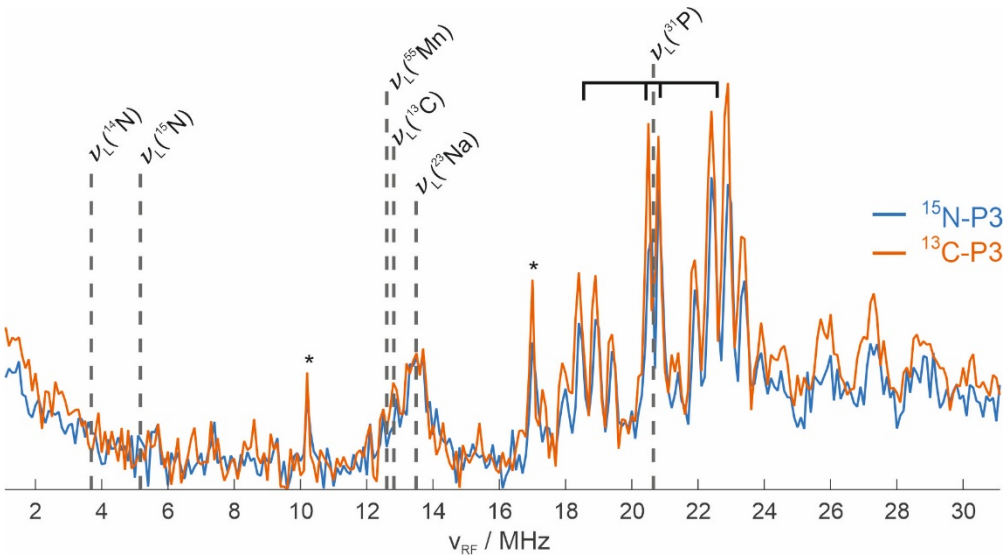


Figure S32. Q-band Mims Chirp ENDOR spectrum with τ = 1 µs and chirped RF excitation (20 µs chirp RF pulse with 100 kHz bandwidth, 2 µs rise time of quarter sine edges). Two separate ^{31}P couplings can be distinguished (annotated with brackets); the peaks of the larger coupling show the blind spot pattern intrinsic to the Mims ENDOR experiment. The peptides used were (^{15}N)VAQAQIN(^{13}C)I-NH_2 and (^{13}C)VAQAQIN(^{15}N)I-NH_2 denoted by ^{15}N-P3 and ^{13}C-P3. ν_L denotes the Larmor frequency. Artefacts marked with an asterisk (*) are due to amplifier overtones exciting the proton Larmor frequency at 51 MHz, which become visible at long acquisition times.

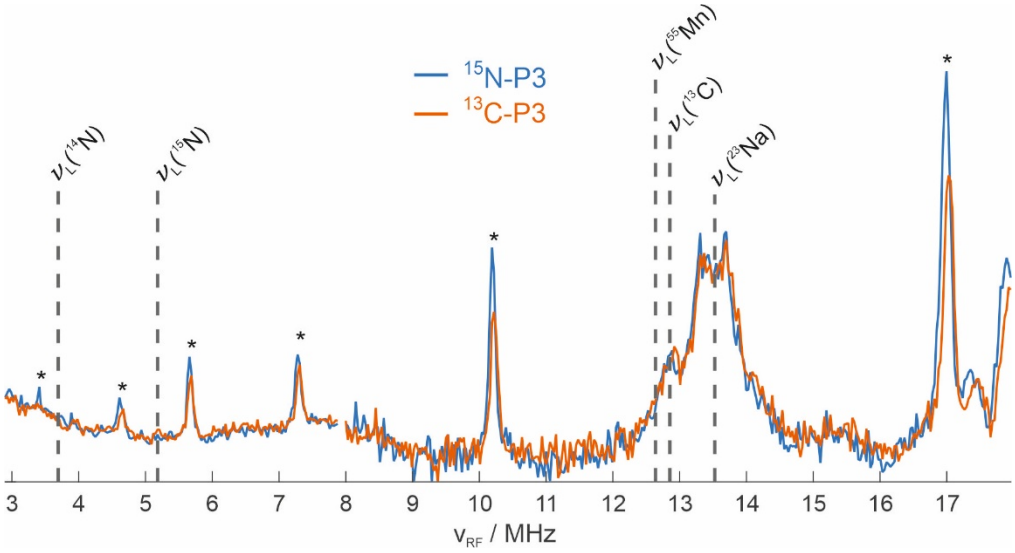


Figure S33. Q-band Mims ENDOR spectrum in the $^{15/14}$N & ^{13}C frequency region. The low-frequency region (<8 MHz) is averaged for longer to increase the S/N-ratio; the intensities stay comparable due to normalization by the number of scans. A small ^{13}C peak on the left shoulder of the ^{23}Na peak is visible. The peptides used were (^{15}N)VAQAQIN(^{13}C)I-NH_2 and (^{13}C)VAQAQIN(^{15}N)I-NH_2 denoted by ^{15}N-P3 and ^{13}C-P3. ν_L denotes the Larmor frequency. Artefacts marked with an asterisk (*) are due to amplifier overtones exciting the proton Larmor frequency at 51 MHz that become visible due to long acquisition time.

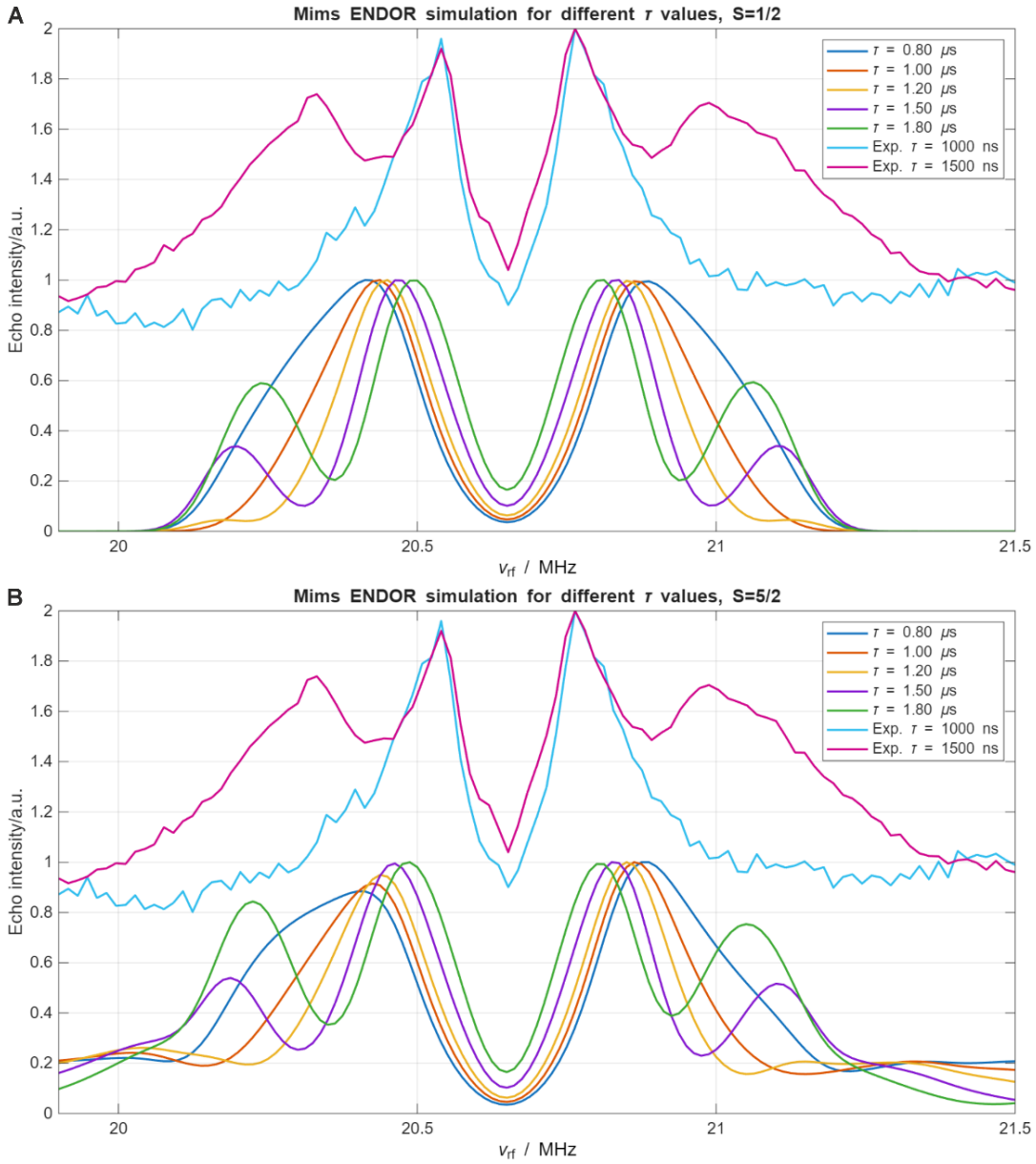


Figure S34. Q-band ^{31}P Mims ENDOR of ^{15}N-P3 with a 40 µs rectangular, monochromatic RF pulse and two different τ values, focusing on the small coupling of around 400 kHz, together with Mims ENDOR simulations for electron spin *S*=1/2 (**A**) and *S*=5/2 (**B**). The simulations based on spin systems with an electron spin (with ZFS for **B**) coupled to a single ^{31}P nucleus with an anisotropic hyperfine coupling of (0 1 0.4) MHz, as an example, show that here a single ^{31}P nucleus is sufficient to produce outer shoulders similar to the experimentally observed spectral line shape.

Table S1: Amyloidogenic peptides used in this study

No.	Composition [a]	Ionization at neutral pH [b]			
		N	Sidechain	C	Sum
1	VFEFEFKFK	+	- - + +	-	0
2	AFEFEFKFK	+	- - + +	-	0
3	DFEFEFKFK	+	- - - + +	-	-1
4	GFEFEFKFK	+	- - + +	-	0
5	FEFEFKFK	+	- - + +	-	0
6	VFEFEFQFQ	+	- -	-	-2
7	FEFEFQFQ	+	- -	-	-2
8	VAQAQINI-NH_2	+			+1
9	AAQAQINI-NH_2	+			+1
10	DAQAQINI-NH_2	+	-		0
11	GAQAQINI-NH_2	+			+1
12	VAQAQINI	+		-	0
13	FQFQFNFN	+		-	0
14	FQFQFNFN-NH_2	+			+1
15	(Orn)QFQFNFN	+	+	-	+1
16	(Orn)QFQFNFN-NH_2	+	+		+2
17	FQFQFQFV-NH_2	+			+1
18	FQFQFQFA-NH_2	+			+1
19	FQFQFQFD-NH_2	+	-		0
20	FQFQFQFG-NH_2	+			+1
21	FVFQFQFV-NH_2	+			+1
22	FAFQFQFA-NH_2	+			+1
23	FEFQFQFE-NH_2	+	- -		-1
24	FGFQFQFG-NH_2	+			+1

[a] Amino acids are represented in the standard single-letter code; Orn is for Ornithine, and –NH_2 is for amidated C-terminus.

[b] Dominant ionization states of the ionizable groups of the peptide at neutral pH are listed as the charges on the N-terminus, side chains, and C-terminus. The listed ionization states are based on the individual pK_a values of the groups and are expected to vary depending on buffer pH and the aggregation state of the peptide.

Table S2: Overview of the experimental parameters used for the solid-state NMR experiments. For more details about the used adiabatic cross-polarization (CP) steps and the tangential shapes used, see reference [6]. All peptide samples used for the solid-state NMR experiments were C-terminally amidated.

Sample	**VAQAQINI:ATP**	**VAQAQINI:ATP**	**VAQAQINI:ATP**
experiment	**^{1}H-^{31}P CP**	**^{31}P DP**	**^{13}C-^{13}C DARR**
ν_r / kHz	17.0	17.0	17.0
B_0/ T	11.7	11.7	16.4
transfer I	^{1}H-^{31}P CP	-	^{1}H-^{13}C CP
ν_1(^{1}H) / kHz	57.2	-	60.0
ν_1(X) / kHz	63.7	-	46.0
shape	tangent ^{1}H	-	tangent ^{1}H
time / ms	1.25	-	1.5
Transfer II	-	-	DARR
ν_1(^{1}H) / kHz	-	-	17.0
time / ms	-	-	20.0
t_1 increments	-	-	2560
spectral width (t_1) / kHz	-	-	100.0
acquisition time (t_1) / ms	-	-	12.8
t_2 increments	2048	16016	3072
spectral width (t_2) / kHz	100.0	100.0	100.0
acquisition time (t_2) / ms	10.2	80.0	15.4
decoupling sequence	Spinal64	Waltz64	Spinal64
^{1}H decoupling power	90.0	5.0	90.0
repetition time / s	2.5	6	2.7
number of scans	4096	10240	24

Table S2 continued:

Sample	**VAQAQINI:ATP**	**VAQAQINI:ATP**	**VAQAQINI:ATP**
experiment	**200 µs ^{15}N-^{31}P NHHP - backbone**	**200 µs ^{15}N-^{31}P NHHP – N-term**	**200 µs ^{13}C-^{31}P CHHP**
ν_r / kHz	17.0	17.0	17.0
B_0/ T	11.7	11.7	11.7
transfer I	^{1}H-^{15}N CP	^{1}H-^{15}N CP	^{1}H-^{13}C CP
$\nu_1(^{1}H)$ / kHz	42.0	42.0	60.0
$\nu_1(X)$ / kHz			43.8
shape	tangent ^{1}H	tangent ^{1}H	tangent ^{1}H
time / ms	0.5	0.75	1.25
Transfer II	^{15}N-^{1}H CP	^{1}H-^{15}N CP	^{1}H-^{13}C CP
$\nu_1(^{1}H)$ / kHz	42.0	42.0	60.0
$\nu_1(X)$ / kHz			43.8
shape	tangent ^{1}H	tangent ^{1}H	tangent ^{1}H
time / ms	0.5	0.75	1.25
Transfer III	^{1}H-^{31}P CP	^{1}H-^{31}P CP	^{1}H-^{31}P CP
$\nu_1(^{1}H)$ / kHz	60.0	60.0	60.0
$\nu_1(X)$ / kHz	36.7	43.8	44.6
shape	tangent ^{1}H	tangent ^{1}H	tangent ^{1}H
time / ms	1.0	1.5	1.5
t_1 increments	64	64	96
spectral width (t_1) / kHz	8.1	8.6	25.0
acquisition time (t_1) / ms	3.9	3.7	1.9
t_2 increments	3072	3072	2048
spectral width (t_2) / kHz	100.0	100.0	100.0
acquisition time (t_2) / ms	10.2	15.4	10.2
decoupling sequence	Spinal64	Spinal64	Spinal64
^{1}H decoupling power	90.0	90.0	90.0
repetition time / s	2.7	2.7	2.7
number of scans	2048	2048	2560

Table S2 continued:

Sample	**VAQAQIN(^{13}C)I : ADP : AcP**	**VAQAQIN(^{13}C)I : ADP : AcP**	**VAQAQIN(^{13}C)I : ADP : AcP – refilled**
experiment	**^{1}H-^{13}C CP**	**^{31}P DP**	**^{1}H-^{31}P CP**
ν_r / kHz	17.0	17.0	17.0
B_0/ T	11.7	11.7	11.7
transfer I	^{1}H-^{13}C CP	-	^{1}H-^{31}P CP
ν_1(^{1}H) / kHz	60.0	-	60.0
ν_1(X) / kHz	41.7	-	42.4
shape	tangent ^{1}H	-	tangent ^{1}H
time / ms	1.25	-	1.0
t_2 increments	3072	16348	3072
spectral width (t_2) / kHz	100.0	100.0	100.0
acquisition time (t_2) / ms	15.4	81.9	15.4
decoupling sequence	Spinal64	Waltz64	Spinal64
^{1}H decoupling power	90.0	5.0	90.0
repetition time / s	1.5	2.5	2.0
number of scans	8	128	3072

Table S2 continued:

Sample	**VAQAQIN(^{13}C)I : ADP : AcP – 5 days**
experiment	**^{31}P DP**
ν_r / kHz	17.0
B_0/ T	11.7
t_2 increments	16348
spectral width (t_2) / kHz	100.0
acquisition time (t_2) / ms	81.9
decoupling sequence	Waltz64
^{1}H decoupling power	5.0
repetition time / s	5
number of scans	4096

Table S3. Restraint and structure statistics

System for structure calculation	
Peptide molecules	10 × VAQAQINI
ATP molecules	1
Layers	5 (2 peptides per layer)
Symmetry restraints	Identical conformation of the 10 peptides
Restraints	
Distance restraints:	
Total	648 (with 2140 ambiguous assignments)
Peptide-peptide	520 (with 1990 ambiguous assignments)
Peptide-ATP	16 (with 38 ambiguous assignments)
Hydrogen bond restraints	112 (2 per hydrogen bond)
Torsion angle restraints	120 (60 ϕ, 60 ψ)
Structure statistics	Mean ± s.d. over 10 conformers
CYANA target function value	5.47 ± 0.42 $Å^2$
Distance restraint violations:	
Number > 0.2 Å	7 ± 2
Maximal violation	0.30 ± 0.0 Å
Torsion angle restraint violations:	
Number > 5°	4 ± 2
Maximal violation	7.35 ± 0.79 Å
RMSD to mean for peptides (residues 1-8):	
Backbone atoms N, C^{α}, C' of all peptides	0.16 ± 0.03 Å
Heavy atoms of all peptides	0.74 ± 0.11 Å
Ramachandran plot statistics (residues 2-7)	100% in most favored region

Supplementary References

1. Kuipers, B. J. H. & Gruppen, H. Prediction of Molar Extinction Coefficients of Proteins and Peptides Using UV Absorption of the Constituent Amino Acids at 214 nm To Enable Quantitative Reverse Phase High-Performance Liquid Chromatography−Mass Spectrometry Analysis. *J. Agric. Food Chem.* **55**, 5445–5451 (2007).
2. Rout, S. K., Rhyner, D., Greenwald, J. & Riek, R. Chapter Four - Characterization of self-templating catalytic amyloids. in *Methods in Enzymology* (ed. Korendovych, I. V.) vol. 697 51–75 (Academic Press, 2024).
3. Rout, S. K. *et al.* An Analysis of Nucleotide–Amyloid Interactions Reveals Selective Binding to Codon-Sized RNA. *J. Am. Chem. Soc.* **145**, 21915–21924 (2023).
4. Stropp, J., Wili, N., Nielsen, N. C. & Klose, D. Increased sensitivity in electron–nuclear double resonance spectroscopy with chirped radiofrequency pulses. *Magn. Reson.* **6**, 33–42 (2025).
5. Tschaggelar, R. *et al.* Cryogenic 35GHz pulse ENDOR probehead accommodating large sample sizes: Performance and applications. *J. Magn. Reson.* **200**, 81–87 (2009).
6. Hediger, S., Meier, B. H., Kurur, N. D., Bodenhausen, G. & Ernst, R. R. NMR cross polarization by adiabatic passage through the Hartmann—Hahn condition (APHH). *Chem. Phys. Lett.* **223**, 283–288 (1994).